NAIC-ID(RS)T-0513-95

NATIONAL AIR INTELLIGENCE CENTER

THERMAL BLOOMING, IODINE LASER TRANSMITTANCE, AEROSOL ABSORPTION, ANISOPLANATISM IN ADAPTIVE OPTICS, AND VERIFICATION OF GROUND-BASED LASER TESTING
(Selected Articles)

Approved for public release: distribution unlimited

DISCLAIMER NOTICE

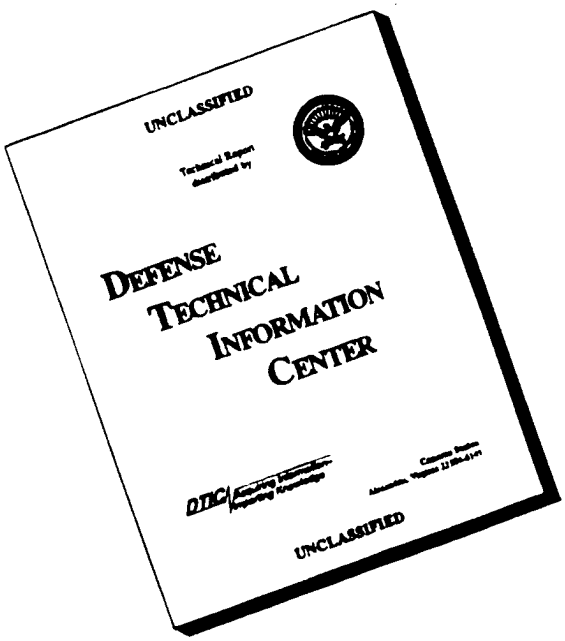

THIS DOCUMENT IS BEST QUALITY AVAILABLE. THE COPY FURNISHED TO DTIC CONTAINED A SIGNIFICANT NUMBER OF PAGES WHICH DO NOT REPRODUCE LEGIBLY.

HUMAN TRANSLATION

NAIC-ID(RS)T-0513-95 8 December 1995

MICROFICHE NR: 95C000760

THERMAL BLOOMING, IODINE LASER TRANSMITTANCE, AEROSOL ABSORPTION, ANISOPLANATISM IN ADAPTIVE OPTICS, AND VERIFICATION OF GROUND-BASED LASER TESTING (Selected Articles)

English pages: 74

Source: Qiangjiguang Yu Zizishu (High Power Laser and Particle Beams), Vol. 5, Nr. 4, November 1993; pp. 521-532; 540-556; 601-607

Country of origin: China
Translated by: Leo Kanner Associates
F33657-88-D-2188
Requester: NAIC/TATD/Bruce Armstrong
Approved for public release: distribution unlimited.

PREPARED BY:

TRANSLATION SERVICES
NATIONAL AIR INTELLIGENCE CENTER
WPAFB, OHIO

TABLE OF CONTENTS

GRAPHICS DISCLAIMER

All figures, graphics, tables, equations, etc. merged into this translation were extracted from the best quality copy available.

EXPERIMENTAL OBSERVATION OF SMALL-SCALE THERMAL-BLOOMING INSTABILITY

Zhang Kai, Shi Jiangjun, Chen Junyan, Qiu Fumin,
Yue Zhengpu, and Yang Chenglong

Southwest Institute of Fluid Physics
P. O. Box 523, Chengdu 610003

ABSTRACT The experimental simulation results of instability of Stimulated Thermal Rayleigh Scattering (STRS) are reported in the paper, which include the studies on the process of instability of the sinusoidal perturbation source propagating in the thermal-blooming medium and the experimental studies on the increase of the small-scale thermal-blooming instability under different perturbation frequencies and different light power, and thus proves that the small-scale instability caused by thermal-blooming increases exponentially as laser propagation in the absorbing medium.

KEY WORDS laser beam propagation in the atmosphere, thermal-blooming, small-scale thermal-blooming instability.

I. Introduction

In 1986, Jan Hermann was the first to discover rapid growth in small-scale thermal-blooming instability during laser transmission in computer simulation. Thereafter, theoretical and experimental studies on small-scale instability became the focus of thermal-blooming research [1-7]. Small-scale instability includes stimulated Rayleigh-scattering (STRS) instability,

stimulated thermal-Brillouin scattering (STBS) instability, and phase-complement instability (PCI). In the period of 1989 to 1990, Lincoln Laboratories, the Northeast Research Conference, and the Livermore National Laboratory reported the rapidly growing phenomena of PCI and STRS instabilities. Researchers generally consider that the probability of small-scale instability may be the final limiting condition of threshold value of transmission intensity of high-powered lasers in the atmosphere with respect to the reflective surface of high-powered lasers with large aperture and short wavelength.

This paper reports that the authors utilized an argon ion laser (single wavelength with maximum output power 1.5W) to simulate thermal-blooming cells by a carbon tetrachloride and iodine solution. The experimental results of rapidly growing perturbation bands of intermediate and small spacing scales in the thermal-blooming formation process are presented. Experimentally, the existence of small-scale instability was proven. Moreover, some experimental studies were conducted on the growing role of small-scale instability at different light power and different perturbation-spacing frequencies.

II. Principle of, and Optical Path, in the Experimental System

Fig. 1 shows the principle of the experimental system. In the experiment, the wavelength of the argon ion laser is 0.488mum, operating at a single wavelength. The output power is continuously adjustable. When the output power is relatively

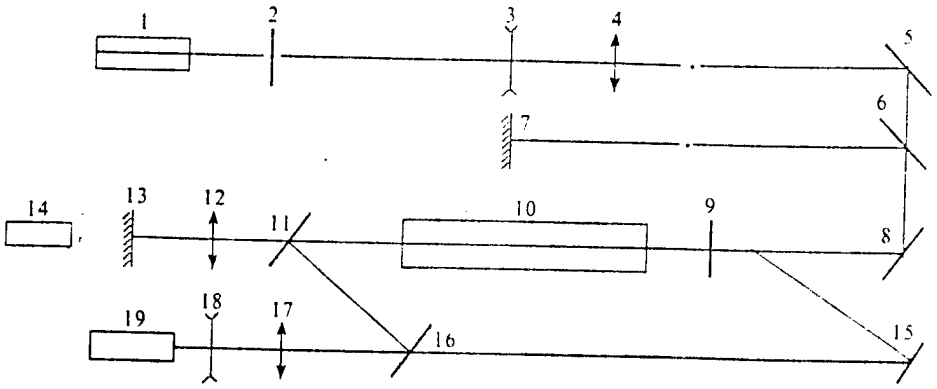

Fig. 1 Layout of the STRS experiment

1. argon－ion laser ; 2. shutter ; 3, 4, 17, 18. beam expension mirrors ; 5, 8. reflectors
6. filtter ; 7. screen 1 ; 9. pertubation source ; 10. thermal－blooming cell
11, 16. beam spliter ; 13. sereen 2 ; 14. CCD camera ; 19. He－Ne laser

small, the output mode is single fundamental mode (TEMsub00). The diameter of the thermal blooming cell is 9cm; its length is 60 or 120cm.

The thermal blooming medium is carbon tetrachloride. The absorption coefficient of a light beam passing through the thermal blooming cell can be controlled by adding small amounts of iodine. The result of growing small-scale instability of thermal blooming was recorded with a high-speed camera and a CCD solid-state camera. After being gathered by the image collecting system, the experimental data were processed on a computer. The fastest sampling frequency of the high-speed camera is 144 frames per second. The CCD real-time image collecting system collects 32 frames of 128x128 images (or 8 frames of 256x256 images) at a speed of 16.6 frames per second. The sampling time of the CCD camera is controlled with an electronic shutter; the shutter

light integration time is 1/10,000-th of a second. The beam expansion lens complex adopts the composition of positive and negative lenses in order to adjust the size of the optical light spots and the straightening properties of the output light spots.

The small-scale perturbation source is realized with two optical glass plates with a certain angle between the two surfaces. The perturbation source is situated in front of the input window of the thermal-blooming cell. After the laser beam passes through the perturbation source and is reflected by two surfaces of the glass plates, the beam interferes with the main laser beam, generating perturbation bands with a distribution of a certain sinusoidal intensity. The spacing period of the band can be adjusted by the angle included between two surfaces of the optical glass plates, and the placement of the band in the optical path.

Experimental light path: after the output of the argon ion laser, the motorized shutter controls the light exposure synchronization and the exposure time, for synchronizing with the CCD camera and the image collection system. After beam expansion of the laser beam through the lens complex, it becomes a straightened beam. After passing through the perturbation source, the beam passes through a thermal-blooming simulation cell. In the exit optical path an imaging lens is placed to converge the light intensity images at the exit of the thermal blooming cell, to form an image on screen 1, then the image is recorded with the high-speed camera or CCD camera system. In the

experiment, another beam of the He-Ne laser is expanded in the reverse direction and passes through the thermal blooming cell. A filter plate isolates the He-Ne laser in the main optical path to be projected onto screen 2. The beam interferes with another beam of reference light for interference measurements for observation of the stability of the carbon tetrachloride solution in the thermal-blooming cell. The observation coefficient of the thermal blooming cell with respect to the argon ion laser beam is obtained by measuring the power at the entrance and exit of the thermal blooming cell with a laser wattmeter.

III. Experimental Parameters and Experimental Results

1. Typical experimental conditions:

laser wavelength λ=0.488micrometer;

absorption coefficient α=0.05cm^{-1};

laser output power P=366mW;

perturbation period (of small-scale perturbation source) d=0.0864cm;

after laser diffusion, light-spot diameter ($1/e^2$), D=0.68cm;

thermal-blooming cell length L=60cm;

initial perturbation intensity $\Delta I/I \approx \pm 0.08$

2. Calculation of parameters

Fennell number (of the entire beam) $N_f = \frac{\pi D^2}{4\lambda Ln} = 83.8$, $n = 1.48$

for small-scale perturbation, the spacing frequency

$$N_p = \frac{\pi d^2}{4\lambda Ln} = 1.35$$

small-scale Fennell number

for laser beam passing through thermal-blooming cell, the irradiation $I_0 = \frac{P}{\pi a^2} = 1.00 \times 10^{-4} \mathrm{W/m^2}$

for laser beam transmission in the CCl_4 solution, the thermal response $\Gamma = \Gamma^* \alpha I_0 = 7.00 \times 10^{-6} \mathrm{s^{-1}}$

in the equation, Γ^* is the thermal response coefficient,

$$\Gamma^* = 1.4 \times 10^{-4} \mathrm{cm^3/J}$$

thermal-blooming growth rate $N_t = \frac{\Gamma Ln}{\lambda} = 12.76 \mathrm{s^{-1}}$

for small-scale perturbation the characteristic expansion time $T_c = (DK^2)^{-1} = 0.234 \mathrm{s}$; $D = \frac{K}{\rho c_p} = 8.1 \times 10^{-4} \mathrm{cm^2/s}$

characteristic expansion length $l_c = \sqrt{D/N_t} = 7.97 \times 10^{-3} \mathrm{cm}$

3. Experimental results

Under the above-mentioned experimental conditions, the authors used the CCD camera and computer data collection system to record the time dependent process of growth in prearranged perturbation of laser light spots and small-scale prearranged perturbation when there is no thermal blooming. At a certain frame frequency, the high-speed camera is used to record the light spot intensity distribution at the exit of the thermal-blooming cell.

During the initial state (t=0, without thermal blooming), the light intensity distribution recorded with the CCD camera is shown in Fig. 2 (sampling points 512x512). From Fig. 2, we can

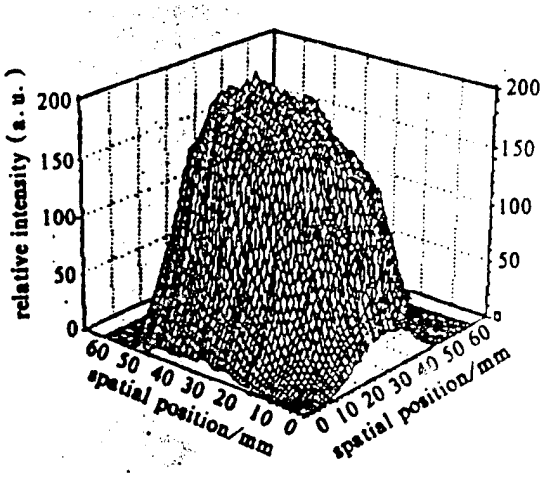

Fig. 2 Spatial distribution of argon-ion laser spot intensity at the thermal-blooming cell exit

see that the light intensity distribution is not the ideal Gaussian distribution due to the effect of fluctuations in laser scattered spots. The contrast of the prearranged perturbation bands is smaller than the estimate based on theoretical calculations. Fig. 3a shows the light spot intensity lines passing through the center line and perpendicular to the perturbation bands when t=0. Fig. 3b through 3f show, respectively, the intensity lines beginning at thermal blooming, then at time intervals 60, 120, 180, 240, and 300ms. At the beginning of thermal blooming, due to the flaw points of the laser scattered spots and the optical system, the prearranged perturbation bands are not distinct. With prolonging of thermal-blooming time, we can see that the contrast of the perturbation bands clearly increases. This proves that during transmission of

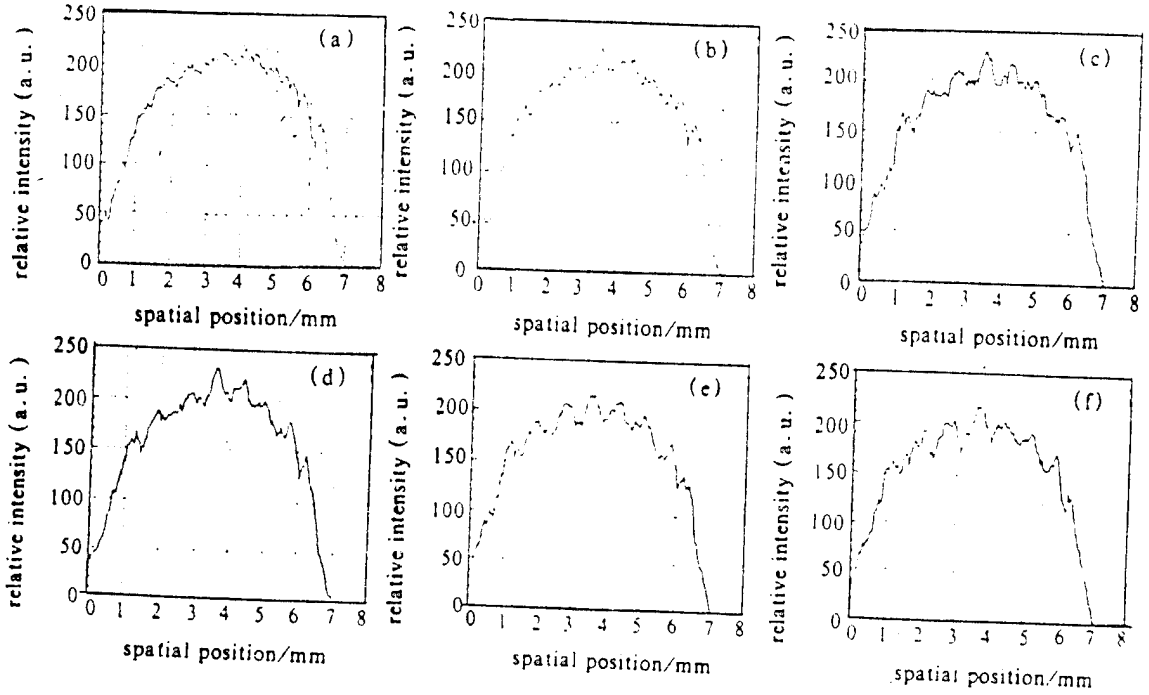

Fig. 3 Intensity distribution at center line at time 0, 60, 120, 180, 240, 300ms

a laser beam in a medium, the small-scale perturbation bands at a certain spacing frequency rapidly grow with the generation of thermal blooming.

Fig. 4a through 4f indicate, respectively, the Fourier transform frequency spectra of light intensity distributions at time 0, and after the beginning of thermal blooming, at time intervals of 60, 120, 180, 240, and 300ms. The corresponding coordinate point of the spacing frequency spectrum of the prearranged small-scale perturbation is $1.3mm^{-1}$. From the corresponding frequency spectral components, we can see the obvious growth in small-scale perturbation bands.

Fig. 5 shows the growth process with time in the spacing

图 3 当时间为0、60、120、180、240、300ms时，中心线上的强度分布

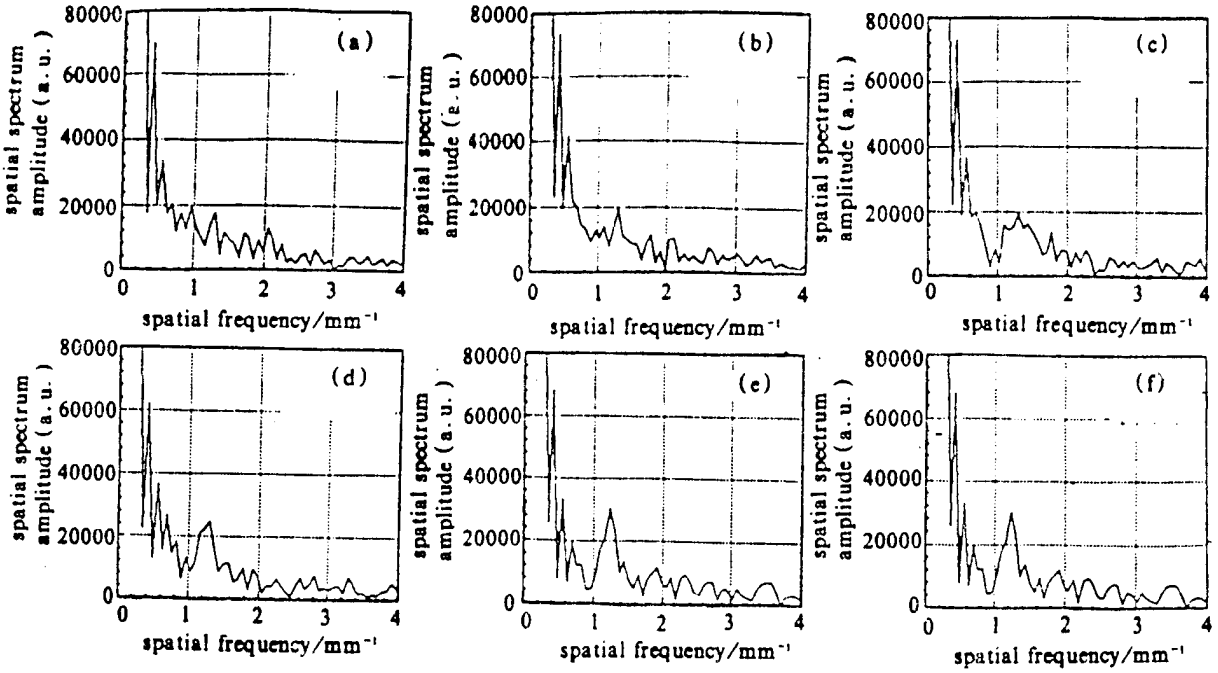

Fig. 4 FFT of the fig. 3

frequency spectral components of small-scale perturbation. Figs. 6a through 6f show a series of pictures of small-scale thermal blooming instability growth at the corresponding intervals.

Moreover, the authors conducted increasing experiments on small-scale perturbation of different laser power and the width of different prearranged perturbation bands. Table 1 shows the experimental conditions and the results. By comparing the experimental results of several experimental conditions, we obtained the following:

1. For the same laser power, for different small-scale perturbation periods, the characteristic time of diffusion is

Table 1 Comparison of the small-scale instability increasing under different experimental condition

	power/mW	perturbation period/cm	$T_r=(D\cdot K^2)^{-1}$/s	$l_r=\sqrt{\frac{D}{N_2}}$/cm	small-scale instability
No.0	366	0.0864	0.234	7.97×10^{-3}	obvious
No.1	184	0.154	0.742	1.12×10^{-2}	obvious
No.2	594	0.069	0.149	6.25×10^{-3}	not obvious
No.3	73	0.154	0.742	1.78×10^{-2}	not obvious
No.4	594	0.108	0.365	6.25×10^{-3}	obvious

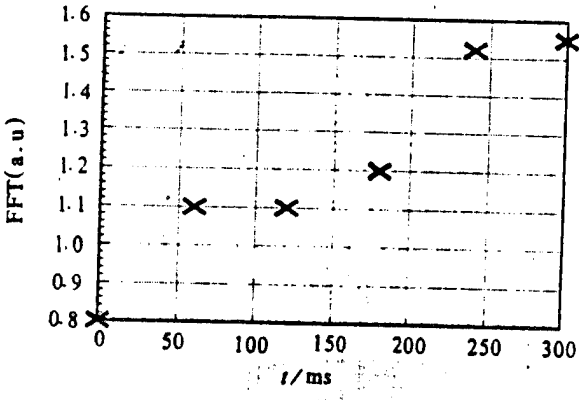

Fig. 5 The small-scale perturbation spatial spectrum amplitude *vs* time
(a) $t=0$ms; (b) $t=60$ms; (c) $t=120$ms; (d) $t=180$ms; (e) $t=240$ms; (f) $t=300$ms

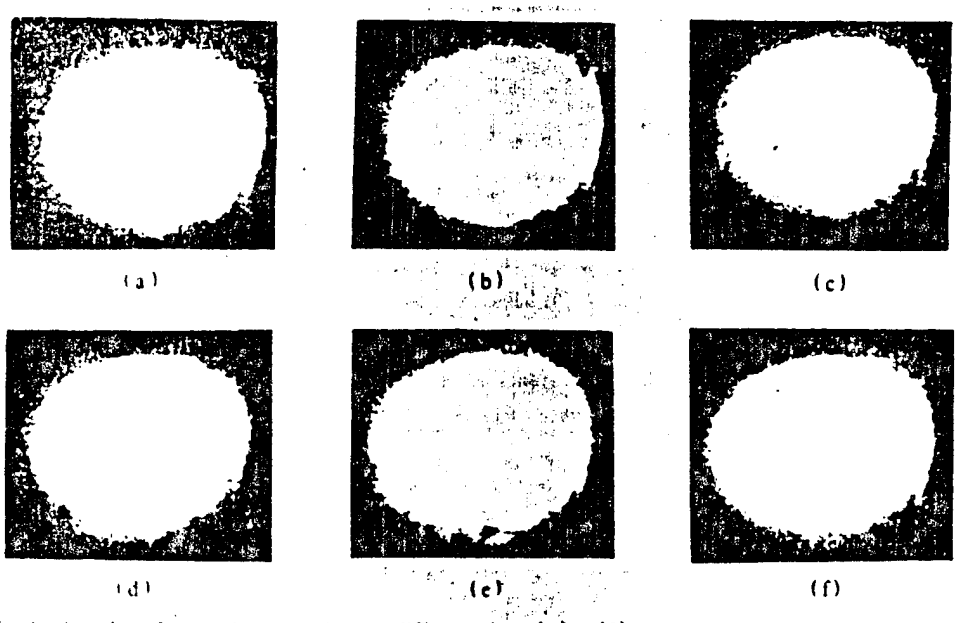

Fig. 6 A series of spot pictures taken at different time (a)~(f) t=0, 60, 120, 180, 240, 300ms

short for small perturbation periods (No. 2). The medium diffusion effect plays a major role, exhibiting the absence of gain for the small-scale. For large perturbation periods (No. 4), the diffusion characteristic time is long. Now the STRS instability grows, playing a major role. This exhibits a clear growth in small-scale prearranged perturbation.

2. For the same small-scale perturbation period, with different laser power, in experiments (No. 1) at large laser power, the small-scale prearranged perturbation bands clearly grow. Conversely (No. 3) for low light power, in this small-scale perturbation spacing period, the diffusion effect of refractivity fluctuations of the medium plays a major role. This shows that small-scale perturbation does not have the phenomenon

of a clearcut growth.

3. The experiment proves that the small-scale spacing perturbation period has a very great effect on the rapid growth in small-scale thermal-blooming instability. This is consistent with the indicator terms in Eqs. (9), that T_c is proportional to the square of K.

4. In the thermal blooming process, whether or not the contrast of small-scale perturbation band intensifies is the competitive result of the diffusion effect that small-scale perturbation rapid growth due to light transmission thermal blooming, and the diffusion effect of the refractivity fluctuations in the medium.

IV. Conclusions

In the small-scale instability experimental studies on open-ring thermal blooming, with an argon ion laser passing through a simulated thermal-blooming cell with carbon tetrachloride and iodine solution, the authors observed the growth of sinusoidal intensity perturbation bands in different experimental conditions. This illustrates that the rapid growth of small-scale perturbations is mainly determined by the growing rate of thermal blooming, and the magnitude of the spacing period of the small spacing scale.

The first draft was received on February 25, 1993; the final revised draft was received for publication on June 1, 1993.

REFERENCES

[1] Frederick G. Gebhardt. Twenty-Five Years of Thermal Blooming: An Overview. *SPIE*, 1990, **1221**: 2~25.

[2] Karr TJ. Measurement of the Stimulated Thermal Rayleigh Scattering Instability. *SPIE*, 1990, **1221**: 328~340.

[3] Ebetein SM. Experimental and Theoretical Investigation of Small-Scale Blooming. *SPIE*, 1990, **1221**: 341~350.

[4] Karr TJ. Thermal Blooming Compensation Instabilities. *J Opt Sot Am*, 1989, A6 (7).

[5] Cambers DH. Linear Theory of Thermal Blooming in Turbulence. Lawrence Livermore National Laboratory Report VCRL-102673. 16 Jun. 1990.

[6] Morris JR. Standard Green's Function Derivation of the Thermal Blooming Compensation Instability Equations. Lawrence Livermore National Laboratory Report VCID-21261. 14 Oct. 1987.

[7] Karr TJ. Instability of Atmospheric Laser Propagation. Lawrence Livermore National Laboratory. *SPIE*, 1990, **1221**.

MEASUREMENTS OF ATMOSPHERIC TRANSMITTANCES FOR 1.315-MICROMETER PHOTOLYTIC IODINE LASER

Yang Gaochao, Han Shouchun, Shao Shisheng,
Hu Ming, Wang Shipeng, and Song Zhengfang

Anhui Institute of Optics and Fine Mechanics,
Chinese Academy of Sciences, P. O. Box 1125,
Hefei, 230031

Cui Tieji, Sun Yizhu, Min Xiangde, and Jing Yuqi

Dalian Institute of Chemistry and Physics,
Chinese Academy of Sciences, P. O. Box 100,
Dalian 116012

ABSTRACT Through actual atmosphere, we have measured atmospheric transmittance for 1.315μm Iodine laser. With medium visibility, relative humidity 64% and 21℃ , average value of atmospheric transmittance is 0.78. This result is fairly identical with computation value obtained by existing data and computer program.

KEY WORDS iodine-laser, atmospheric propagation, atmospheric tranmittance.

I. Introduction

The 1.315-micrometer iodine laser located at the window region of the atmosphere evoked great interest, since it has enormous potential as a high-energy laser. Many specialists conducted research on the laser absorption in laboratories of water vapor, carbon dioxide, methane, and other gaseous molecules

[1-3]. However, to date there have been no experimental studies reported on atmospheric transmittance of iodine lasers. This is a necessary step toward understanding the transmittance of iodine lasers in the atmosphere in order to completely study their application potentials. Therefore, in September and October 1991, the authors conducted experimental studies measuring atmospheric transmittance for the photolytic iodine laser (λ=1.315micrometers) in near-ground horizontal transmission at the Anhui Institute of Optics and Fine Mechanics. The article analyzes the data obtained in the experiment. Moreover, the LASER program was used to confirm the experimental results.

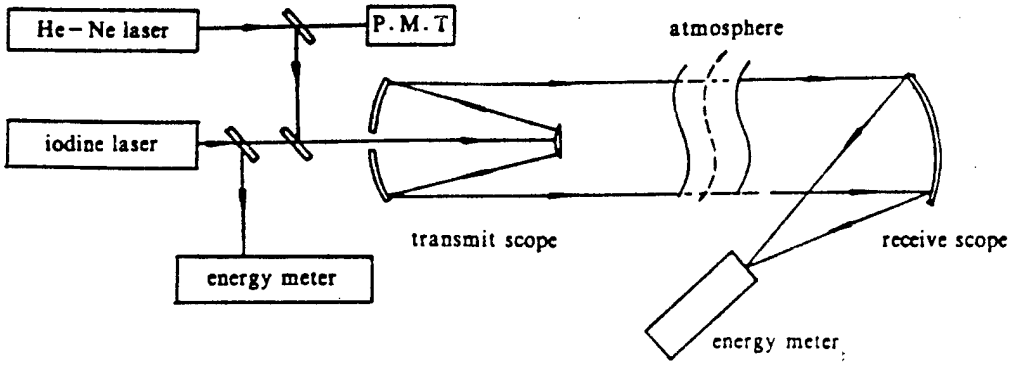

Fig. 1 The schematic diagram of experiment system

II. General Experimental State

Fig. 1 is the schematic diagram of the entire experimental system. The photolytic iodine laser device was developed and provided by the Dalian Institute of Chemistry and Physics of the

Chinese Academy of Sciences. The pulse width of the laser was 100microseconeds, since the outputted laser beam was of ring-shaped low-order mode. The exterior diameter of the ring-shaped light beam was 18mm, and the outputted laser energy was 80mJ. In addition to its use as light guidance, the He-Ne laser was also used as a light source to measure the atmospheric transmittance of the 0.6328-micrometer laser. The atmospheric transmittance of the wavelength was used to estimate the extinction coefficient of the atmospheric aerosol particles in the total experimental light path. However, lasers at both wavelengths were transmitted through a Cassegrain telescope with an aperture 3mm OD. At the receiving end, there was an aluminum coated concave mirror (m=1m) with OD 290mm. After convergence of the received laser beam, a laser wattmeter was used to conduct detection of 1.15-micrometer laser energy. The 0.6328-micrometer laser signal was detected with a photomultiplier tube. To obtain the real-time data of atmospheric transmittance, synchronous monitoring was conducted at the transmission terminal on the laser transmission energy or power of both wavelengths by using the laser wattmeter and a photomultiplier tube. To ensure data reliability, before and after measurement experiments each day, comparative calibration of the system was made on the instruments at both terminals. By definition, the calibrated coefficient of the system multiplied by the ratio of the measured values between the receiving end and the transmission end is the actual atmospheric transmittance of the transmission light path.

The transmission distance between the transmission end and the receiving end of this experiment was 0.46km. Although it was mid-autumn, yet mostly cloudy during the experimental period, with frequent drizzly or foggy days. The relative humidity was between 60 and 80%. There were rarely sunny days. To ensure the correct processing of the experimental data, the authors made observations in the entire experimental period as well as to the conventional meteorological parameters (such as temperature, relative humidity, atmospheric pressure, and visibility in the atmosphere).

III. Data Processing

During laser transmission in the atmosphere, before the emergence of the nonlinear effect, the transmittance can be described with

$$T = \exp[-\int_0^L \mu(r)dr] \qquad (1)$$

which is Lambert's law. In the optical path of horizontal transmission, the atmospheric medium in the optical path can be considered as a homogeneous medium. Therefore,

$$T = \exp[-\mu L] \qquad (2)$$

In Eq. (2), L is the transmission distance; and μ is the attenuation coefficient of the atmospheric medium. The coefficient includes the absorption coefficient α_m and the scattering coefficient $beta_m$ induced by absorption and scattering

by the gas molecules in the atmosphere, as well as the extinction coefficient due to absorption and scattering of the aerosol particles in the atmosphere. That is, the attenuation coefficient

$$\mu = \alpha_m + \beta_m + \beta_p \qquad (3)$$

In actual atmospheric transmission of the 1.315-micrometer iodine laser, besides the aerosol particle scattering, absorption by water vapor molecules in the atmosphere is the main factor affecting transmittance. There are other atmospheric gas particles (such as carbon dioxide, methane, and ammonia) also making a certain contribution to the atmospheric transmission attenuation of the iodine laser wavelength. However, this is a small quantity compared to the absorption of water vapor molecules. Therefore, in this article, we do not consider, for the time being, the attenuation function for a 1.315-micrometer laser absorbed and generated by these gas molecules. During data processing, the functions due to these gas molecules are also considered as the absorption coefficient of atmospheric molecules. At the 1.315-micrometer wavelength, the molecule scattering coefficient is relatively small and can be neglected.

In actual atmospheric transmission of an iodine laser, the main function affecting the transmittance is scattering of the atmospheric aerosol particles, and absorption by the atmospheric molecules. In the authors' experiments, the atmospheric transmittance of the iodine laser obtained can be written as

$$T_r = \exp[-(\alpha_m + \beta_p)L] \qquad (4)$$

Here we neglect the molecule scattering coefficient β_m at the 1.315-micrometer wavelength.

With respect to the radiation transmission, by using the scattering of atmospheric aerosol particles as the main light extinction factor, generally the following empirical formula is used to estimate the extinction coefficient.

$$\mu = (3.912/V_M)(0.55/\lambda)^q \qquad (5)$$

In the equation, V_M is atmospheric visibility (km); λ is the radiation wavelength (micrometers); and q is the visibility-wavelength revision factor.

$$q = \begin{cases} 0.585V_M^{1/3} & V_M < 6\text{km} \\ 1.3 & 6\text{km} \leq V_M \leq 20\text{km} \\ 1.6 & V_M > 20\text{km} \end{cases} \qquad (6)$$

The effectiveness of Eq. (5) has been proven by a series of experiments by the authors [4]. The attenuation of an He-Ne laser for λ=0.6328micrometers is the result of the scattering function of the atmospheric aerosol particles. However, the absorption and other functions of the atmospheric gaseous molecules can be neglected. Therefore, we can use the atmospheric transmittance of the 0.6328-micrometer laser, and estimate the extinction coefficient for scattering by the atmospheric aerosol particles with Eq. (5). If in the experiments the atmospheric transmittance is T_H for the 0.6328-micrometer laser, and the scattering coefficient for the aerosol

particles is β_{ph}, then we can obtain the following from Eqs. (2), (5), and (6)

$$\beta_{p,II} = -(\ln T_{II})/L = (3.912/V_M)(0.55/0.6328)^q \qquad (7)$$

By substituting λ=1.315micrometers into Eq. (5), with some manipulation we can obtain the scattering coefficient of the iodine laser for the aerosol particles as

$$\beta_{I,p} = \beta_{p,II}(0.6328/1.315)^q = -[(\ln T_{II})/L](0.4812)^q \qquad (8)$$

Substitute Eq. (8) in Eq. (4) and we have

$$T_I = \exp[-(\alpha_m + \beta_{I,p})L] = \exp\{-[\alpha_m - 0.4812^q(\ln T_{II})/L]L\} \qquad (9)$$

T_I is the atmospheric transmittance of an iodine laser in actual measurement. Thus we can obtain the absorption coefficient of the iodine laser due to the atmospheric molecules as

$$\alpha_m = [(0.4812)^q \ln T_{II} - \ln T_I]/L \qquad (10)$$

During the horizontal atmospheric transmission (L=0.46km) of the iodine laser, the atmospheric transmittance T (km^{-1}) can be written as

$$T = \exp\{-[(-\ln T_{II})/0.46]\} \qquad (11)$$

When we consider the transmittance T' (km^{-1}) during the absorption of atmospheric molecules, the following equation can be used to describe the transmittance:

$$T' = \exp\{[0.4812^q \ln T_I - \ln T_{II}]/0.46\} \qquad (12)$$

In the equation, the value of q is determined by (6)

IV. Results and Discussion

Table 1 lists some of the typical data, including the atmospheric transmittances (T_H and T_I) measured at the distance of 460m for an He-Ne laser and an iodine laser. Derived from Eqs. (11) and (12), the atmospheric transmittance of the iodine laser per km (T) and the per-km transmittance (T') in the situation of absorption by molecules, with deduction of the aerosol extinction coefficient, we obtain the molecule absorption coefficient α_m. The first three columns are the visibility V_M, relative humidity (H), and temperature (t).

From the data in Table 1, we can see the following: during

Table 1 The typical measurement results of atmospheric transmittance for iodine laser (1991.10)

Date 91 – 10	Time	V_M/ km	H/ %	t/ ℃	T_M	· T_I	T/ km^{-1}	T'/ km^{-1}	α_m/ km^{-1}
6	09 : 30	7.0			0.800	0.878	0.754	0.909	0.095
	09 : 30	7.0			0.800	0.863	0.727	0.876	0.132
	09 : 30	7.0			0.800	0.869	0.736	0.888	0.119
7	15 : 10	7.0			0.800	0.850	0.701	0.846	0.167
	15 : 15	7.0			0.800	0.905	0.806	0.972	0.029
	15 : 30	7.0			0.800	0.888	0.772	0.932	0.071
	15 : 40	7.0			0.800	0.864	0.729	0.879	0.129
	15 : 53	7.0			0.800	0.840	0.685	0.827	0.190

Date 91－10	Time	V_M/km	H/%	t/℃	T_H	$\cdot T_t$	T/km^{-1}	T'/km^{-1}	α_m/km^{-1}
8	14:46	15.0	61	22	0.870	0.903	0.801	0.900	0.105
	14:51	15.0	60	22	0.870	0.931	0.857	0.963	0.037
	15:05	15.0	60	22	0.870	0.921	0.836	0.939	0.063
	15:14	15.0	60	22	0.870	0.933	0.860	0.967	0.034
	16:00	15.0	61	21.5	0.870	0.928	0.850	0.956	0.045
	16:08	15.0	62	21.5	0.870	0.909	0.813	0.914	0.090
	16:12	15.0	62	21.5	0.870	0.934	0.862	0.969	0.032
	16:16	15.0	62	21.5	0.870	0.894	0.783	0.880	0.127
	16:20	15.0	62	21.5	0.870	0.920	0.834	0.937	0.065
9	09:06	5.0	76	17.5	0.860	0.870	0.739	0.866	0.144
	09:23	5.0	73	18	0.860	0.865	0.730	0.855	0.157
	10:08	5.0	72.5	18.5	0.860	0.880	0.757	0.886	0.121
	10:25	5.0	71	18.5	0.860	0.900	0.795	0.931	0.072
	14:46	8.0	61	22	0.890	0.900	0.795	0.876	0.132
	14:51	8.0	61	22	0.890	0.908	0.810	0.894	0.113
	15:02	8.0	61	22	0.890	0.902	0.799	0.881	0.127
12	15:10	10.0	64	21	0.880	0.881	0.760	0.846	0.168
	15:38	10.0	63	21	0.880	0.885	0.767	0.854	0.158
	15:44	10.0	64	21	0.880	0.877	0.751	0.836	0.179

atmospheric transmission of a 1.315-micrometer iodine laser, its transmittance varies mainly with the variations in atmospheric visibility and water vapor content. The average meteorological conditions are V_M=10km, H=64%, and t=21°C. For the iodine laser, the average transmittance T=0.78km^{-1}, and the corresponding attenuation coefficient μ=0.246km^{-1}. Among the latter, the molecular absorption coefficient α_m=0.107km^{-1}, and the aerosol extinction coefficient β_p=0.139km-1

To verify the trustworthiness of the above-mentioned results, the authors made computations by using the data of high-resolving-power spectral lines of AFGL in the United States, and the LASER program. Table 2 shows the results. Thus, we know

that if the two types (urban type and rural type) aerosol

Table 2 Calculation results of atmospheric attenuation for 1.315μm iodine laser (V_m=10km)

Climate		tropic	mid-latitude summer	mid-latitude winter	subarctic summer	U.S. standary	text
α_m/ km^{-1}		0.265	0.187	0.042	0.115	0.075	0.155
β_p/ km^{-1}	urban	0.152					
	rural	0.123					
	maritime	0.315					

Climate conditions of the text : t=21℃ , H=64%.

extinction coefficients are averaged up, the calculated β_p=0.137 agrees fully with the experimental value. However, the experimental site was between the urban and rural areas, approximately 10km from the city boundary. The aerosol property should be between the urban and the rural types. The above-mentioned situation means that our processing method is reliable. In other words, the application of atmospheric transmittance of an He-Ne laser to calculate the aerosol extinction function of other laser wavelength is on a reliable basis.

As for the molecular absorption coefficient, the average value is very close to the calculated value, smaller than 30%. There are two possible reasons: one is the shorter transmission distance with low instrumental precision, thus causing certain experimental errors. From the discrepancy of data in Eq. (1), individual data may have deviations of more than 30%. It is possible to have certain deviations when averaging. Secondly,

there are some flaws in the database of the AFGL spectral lines. Generally speaking, the database is reliable but there may be room for improvement due to limitations of technical conditions at that time. In recent years, work in this direction was reported in successive cases. For example, Gao Junyi et al. [5] discovered that the ray intensity and linewidth given by Rilter were on the larger side. However, the results from Grossmann et al. were on the smaller side. If the absorption cross-section ($\sigma_{[illegible]}=1.1\times10^{-24}$ cm_2) of water vapor molecules at the 1.315-micrometer wavelength given by Bragg and Kelly [3] are used to calculate the molecular absorption coefficient at only $0.043km^{-1}$ under the experimental conditions. The value is reduced down to less than half of the AFGL data. Further discussion is necessary to determine which is right and which is wrong.

With this experiment, generally we can obtain the following results: in the fall in the Hefei area, during the horizontal atmospheric optical path transmission of the iodine laser, the variation in atmospheric transmittance is approximately between 70 and 85%. When the temperature is 21°C and the relative humidity is 64%, the absorption coefficient of the atmospheric molecules is approximately $0.11km^{-1}$ for the 1.315-micrometer iodine laser. The main factor affecting atmospheric transmittance of the iodine laser is scattering of the atmospheric aerosol particles, and the varying absorption of water vapor due to variable water content in the atmosphere.

Since the iodine 1.315-micrometer laser is at the far end of the water vapor absorption line, it is very difficult to measure only the water vapor absorption coefficient at this wavelength in the actual atmosphere.

To obtain more accurate transmittance and water vapor coefficient for an iodine laser in actual transmission in the atmosphere, we should make experimental measurements at longer distances. In addition, we should conduct detailed studies in a simulation laboratory on the relationship among temperature, pressure, and water vapor content at the 1.315-micrometer wavelength for the water vapor molecular coefficient. Research in this direction will be pursued when conditions are suitable.

The first draft was received on February 26, 1993. The final revised draft was received on Nay 5, 1993.

REFERENCES

[1] Lawdon SA, and Bragg SL. Photoacoustic Absorption Spectra of Atmospheric Gases near 7603cm^{-1}. *Appl Opt*, 1984, **23**: 3042.

[2] Wiggins TA. Water Vapor Absorption at the Atomic Iodine Laser Line. *Appl Opt*, 1981, **20**: 3481.

[3] Bragg SL and Kelly JD. Atmospheric Water Vapor Absorption at 1.3μm. *Appl Opt*. 1987, **26**: 506.

4. Song Zhengfang, Fundamentals of Applied Atmosphere Optics, Beijing: Qixian Meteorology Publishing House, 1989, p. 52.

5. Gao Junyi et al., "Spectrum Research of High Resolution Oxygen A band," CHINA LASERS, 19/12:938 (1992).

EFFECTIVE ABSORPTION COEFFICIENT OF AEROSOL HEATED BY LASER

Liu Yanyan, Wang Junbo, Le Shixiao,
Yang Xiaoli, and Lin Weigan

Institute of Applied Physics,
University of Electronics, Science and Technology,
Chengdu 610054

ABSTRACT Thermal blooming induced by aerosol is discussed in laser beam propagation though atmosphere. We give the effective absorption coefficient $\alpha_{eff}(t)$. Because of the limited conductivity of air, the increment of temperature of air heated by aerosol absorbing energy from laser beam is imhomogeneous, which lead to the $\alpha_{eff}(t)$ dependent on time. The delay time t_p, when the $\alpha_{eff}(t)$ arrives at the maximum value, is dependent on the radius of aerosol.
KEY WORDS aerosol, high power laser, thermal blooming, effective absorption coefficient.

I. Introduction

In theoretical research on high-powered laser propagation in the atmosphere, at present research on thermal blooming is mainly concentrated on the molecular absorption effects, but neglects the contribution made by aerosol particles to thermal blooming in the atmosphere. If the laser wavelength at the atmospheric window is properly selected, absorption by molecules is very low. Here the effect due to aerosol particles should be considered.

When there is an absence of particle puncture, breaking, or evaporation, G. Caledonia [1] and D. E. Lencloni [2] et al. neglected the relationship of heat exchange between particles and air. It is assumed that all energy of the aerosol particles absorbed from a laser beam is transferred to the atmosphere with no time delay, the effective absorption coefficient of aerosol particles is the absorption coefficient of aerosol particle. C. H. Chan [3] neglected the limited heat conductivity of air; he assumed that some of the energy absorbed by aerosol particles from a laser beam is used to heat particles, and the remainder is converted to heat and is rapidly diffused in the air. Thus, air is uniformly heated thereby inducing the effective absorption coefficient of aerosol particles.

For the real atmosphere, since the coefficient of thermal conductivity of the atmospheric molecules is smaller, the heat entering the air is always first stored in the circumference of the particles, forming a heat well, thus constituting a region with a local temperature gradient prior to outward diffusion. Thus, the heat entering the air does not immediately heat up all the air. Research reported in this paper aims at using the theory of the present-day continuous-operation lasers to heat single aerosol particles, leading to thermal blooming, and to be led into the group of aerosol particles with consideration given to heat exchange between particles and air, as well as the finite thermal conductivity of air. We study the effective absorption coefficient for heating of group aerosol particles caused by a

laser. In the second part of the paper, the authors describe the models and formula used by single particles to heat the surrounding air. In the third part, the authors present the models and formula of the effective absorption coefficient of the heat effect by group aerosol particles. The fourth part presents the theoretical calculations.

II. Air Temperature Distribution Surrounding Single Particles after Heating

For convenience in this discussion, the authors neglect absorption by atmospheric particles. The temperature variation distribution of air surrounding the spherical shaped aerosol particles with uniform absorption can be obtained from Eq. (1) [3-5].

$$\frac{1}{\kappa}\frac{\partial T}{\partial t} = \nabla^2 T \qquad (1)$$

Boundary conditions

$$IQ_{abs}\pi a^2 = -4\pi J a^2 k_a \left(\frac{\partial T}{\partial t}\right)_{r=0} + \frac{4\pi}{3} a^3 J \rho_p c_p \left(\frac{\partial T}{\partial t}\right)_{r=a} \qquad (2)$$

$$T = T_0 \quad \text{when} \quad r = \infty \qquad (3)$$

Initial condition

$$T = T_0 \quad \text{when} \quad t=0 \qquad (4)$$

Here $\kappa = \frac{k_a}{\rho_a c_a}$, κ, k_a, ρ_a, and c_a indicate, respectively, the thermal expansion rate, thermal conductivity, density, and specific heat capacity of air. J is Joule's constant; and a is the radius of aerosol particles. ρ_p and c_p are, respectively, the density and specific heat capacity of the particles. I is

the incident laser intensity. Q_{abs} is the absorption coefficient of aerosol particles to be solved in the theory of Mie scattering. T is temperature and T_0 is the temperature before the action of air and particles. This is under the assumption that air and particles are at the same temperature. In Eq. (2), the authors have assumed that the internal temperature of the particles is uniformly distributed, neglecting the evaporative effect of the particles.

From Eqs. (1) through (4), we can obtain the approximate solution [3,5] of the aerosol particles heated with continuous-waves at a point P (x, y, z) by the particles at any points O(x', y', z') in space.

$$T(r,a;r',t)=T_0+\frac{2a\Delta T_s(a)}{r\sqrt{\pi}}\int_\beta^\infty\{1-\exp[-\frac{t}{\tau(a)}(1-\frac{\beta^2}{\mu^2})]\}\exp[-\mu^2]du \tag{5}$$

Temperatures of particles

$$T_a(t)=T_0+\Delta T_s(a)\{1-\exp[-\frac{t}{\tau(a)}]\} \tag{6}$$

Here $r=|r-r'|$, $\beta=\frac{r-a}{\sqrt{4k_a t}}$, $\Delta T_s(a)=\frac{IQ_{abs}a}{4k_a J}$ is the highest temperature rise that can be attained by aerosol particles with a as the radius. $\tau=\frac{a^2\rho_a c_a}{3k_a}$ is the time constant of the temperature increase of aerosol particles. After a single spherical-shaped aerosol particle absorbs laser beam energy and heats the air (with a as the radius), the air temperature is given by Eq. (5) at time t with distance r from the particle center.

III. Effective Absorption Coefficient of Group Aerosol Particles

The assumption is made that the aerosol particles are distributed with the single dispersion spectrum; the chemical properties and the geometric parameters of all aerosol particles are the same. They are uniformly distributed in air. To simplify the model, particle motion is neglected.

If the density distribution of aerosol particles in air is uniform, then the probability of particle existence in the volume element dx'dy'dz' near O(x',y',z') is dx'dy'dz', therefore the temperature rise of point P(x,y,z) at a distance r from O is $\Delta T(r,a;r',t)$; its probability if dx'dy'dz'. Therefore, the average temperature rise $\Delta\overline{T}$ at any instant can be expressed as [6]

$$\Delta\overline{T}(r,a,t) = N\int_V dx'dy'dz' \frac{2a\Delta T_\tau(a)}{r\sqrt{\pi}} \int_\beta^\infty \{1 - \exp[-\frac{t}{\tau(a)}(1-\frac{\beta^2}{\mu^2})]\}\exp[-\mu^2]\,d\mu \qquad (7)$$

In a unit volume near this point, the heat required to induce an average temperature rise $\Delta\overline{T}$ (r,a,t) of this point at time t is

$$\Delta Q(r,a,t) = Jc_a\rho_a\Delta\overline{T}(r,a,t) \qquad (8)$$

If we assume that thermal blooming of this portion is uniformly absorbed by the atmosphere, the effective absorption coefficient similar to molecular absorption can be used to indicate the thermal blooming inducing the average temperature rise of the atmosphere due to the energy from the laser beam absorbed by the aerosol particles

$$\Delta Q(t) = \int_0^t I(t)\alpha_{eff}(t)dt \qquad (9)$$

Then the effective absorption coefficient of aerosol particles with respect to planar waves is

$$\alpha_{eff}(t) = \frac{c_a \rho_a}{I(t)} \frac{d\Delta T(t)}{dt}$$

$$= \frac{J c_a \rho_a N}{I(t)} \int_v dx'dy'dz' \frac{2a\Delta T_\infty}{r\sqrt{\pi}} \int_\beta^\infty \frac{1}{\tau}\{\exp[-\frac{t}{\tau}(1-\frac{\beta^2}{\mu^2})]\}\exp[-\mu^2]\,d\mu \qquad (10)$$

IV. Calculation Results

It is assumed that the incident laser is planar-wave. We made computations on the effective absorption coefficient of carbon particles and water droplets from a laser incidence to single scattering spectrum with wavelengths λ=3.8micrometers and λ=10.6micrometers. The particle concentrations are N=10/cm^3 and particle radius a=5micrometers. The specific heat capacity (of carbon particles) c_p=0.711J/g·K, ρ_p=2.55g/cm^3. When λ=3.8micrometers, n=1.8-i0.3. When λ=10.6micrometers, n=2.2-i0.9. The specific heat capacity (of water droplets), c_p=4.18J/g·K, ρ_p=1.0g/cm^3. When λ=3.6micrometers, n=1.42-i0.013. When λ=10.6micrometers, n=1.13-i0.08. For air, its heat conductivity k_a=2.54x10^{-4}J/s.cm.K. and its Joule's constant J=4.187J/cal.

Figs. 1 and 2 show the time dependent variation curves of effective absorption coefficient for carbon particles and water

droplets for lasers with different wavelengths. From the figures, we can see the following. The effective absorption

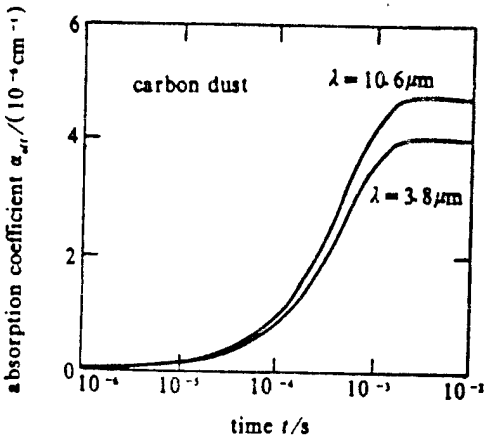

Fig. 1 Effective absorption coefficient α_{eff} for carbon at 3.8μm and 10.6μm

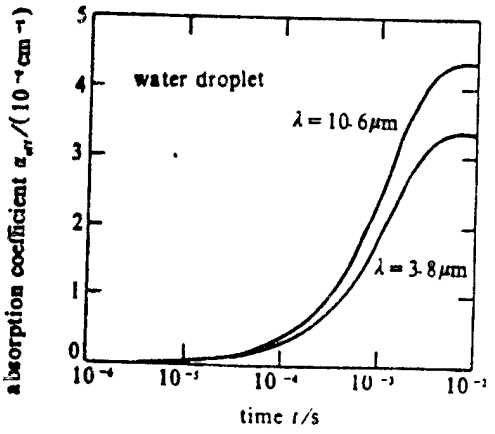

Fig. 2 Effective absorption coefficient α_{eff} for water droplet at 3.8μm and 10.6μm

coefficient is nearly 0 at 0.1microsecond. With prolonging of time, the effective absorption coefficient slowly increases. After a certain time period, the coefficient increases rapidly, until a maximum value is reached. Thereafter, the coefficient decreases slowly, finally arriving at a steady state. Now this is the total absorption coefficient of group aerosol particles. This is a greater difference than the results of absorption by pure molecules. Because after the aerosol particles absorb heat, part of the heat absorbed will be stored internally to form a heat well, and another part of the heat heats the surrounding air. At the beginning, most heat is stored inside the aerosol particles; very little of the heat enters the air so that there

is very small variation of air. Thus, the corresponding effective absorption coefficient is almost zero. As time passes, the temperature rise of particle slows down, and heat entering the air increases. However, due to the finite thermal conductivity of air, the heat is accumulated surrounding the particles, forming a locally inhomogeneous region. Now, the effect on air variation increases. Correspondingly, the effective absorption coefficient begins slowly increasing. Hereafter, heat stored in the inhomogeneous region locally surrounding the particle also begins to diffuse, and the effective absorption coefficient increases rapidly, to a maximum value. Due to the function of diffusion of stored heat and thermal blooming, and the conduction of thermal blooming from particles, this maximum value of the coefficient is slightly greater than the total absorption of the group aerosol particles. With progress of thermal diffusion, local inhomogeneity becomes less and the effective absorption coefficient begins decreasing. Finally, only thermal blooming of particle absorption is functioning.

We define that the emergence time for the maximum value of the effective absorption coefficient is the delay time of effective absorption coefficient of aerosol particles. To solve for Eq. (10), we can obtain the variation rate of the effective absorption coefficient with time.

$$\frac{d\alpha_{eff}(t)}{dt} = \frac{Jc_a\rho_a N}{I(t)} \int_v dx'dy'dz' \frac{2a\Delta T_x}{r\sqrt{\pi}} \{ \frac{\beta}{2t} \exp(-\beta^2) - \int_\beta^\infty \frac{1}{\tau^2} \exp[-\frac{t}{\tau}(1-\frac{\beta^2}{\mu^2})] \exp[-\mu^2] du \} \quad (11)$$

Then, the delay time t_D of the effective absorption coefficient can be obtained from $\frac{d\alpha_{eff}(t)}{dt} = 0$.

$$\int_v dx'dy'dz' \frac{2a\Delta T_x}{r\sqrt{\pi}} \{ \frac{\beta}{2t} \exp[-\beta^2] - \int_\beta^\infty \frac{1}{\tau^2} \exp[-\frac{t}{\tau}(1-\frac{\beta^2}{\mu^2})] \exp[-\mu^2] d\mu \} = 0 \quad (12)$$

Fig. 3 shows the time-dependent curves of the appearance of the maximum value of the effective absorption coefficient due to the

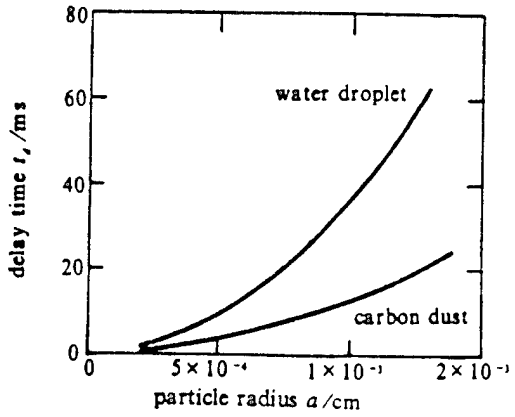

Fig. 3 Delay-time t_p *versus* particle radius a
(1) water droplet; (2) carbon dust

action of a laser for carbon particles and water droplets with different radii. From the figure we can see the following: with

increasing radius, the delay time of maximum value of the effective absorption coefficient increases. This is because the greater the particle radius, the more the temperature rises to reach equilibrium. The longer the characteristic time, the more the heat stored surrounding the particle, therefore the greater the time delay.

IV. Conclusions

In the foregoing, the authors studied the time-dependent variation process of the effective absorption coefficient for an increase in atmospheric mean temperature in the process that aerosol particles have the energy absorbed from laser beams to transfer to air during the interaction between aerosol particles and the laser beam. From the calculation results, we can see the following: in the time range below picoseconds, the effective absorption coefficient of air due to aerosol particles can be neglected. With the time period of picoseconds to submilliseconds, the time-dependent variation in the effective absorption coefficient of air caused by aerosol particles is very complex. In this time period, we should adopt a method differing from molecular absorption in processing. After submilliseconds, the effective absorption coefficient in air (caused by aerosol particles) attains a steady state, not varying with environment. This can be applied directly so that the overall absorption coefficient of aerosol particles can be used to obtain the effective absorption coefficient.

The research was funded by State Project 863 in Laser Technology. The first draft was received on June 9, 1993; the final revised draft was received for publication on August 9, 1993.

REFERENCES

[1] Caledonia G, Teare D. Laser beam atmosphere aerosol interactions. Proc Winter Meeting of A.S.M.E, 1975.

[2] Lencioni DE, Kleiman H. Effects of aerosol particle heating on laser beam propagation. Lincoln laboratory Tech Report LTP-27. 1974, 22 July.

[3] Chen CH. Effective absorption for thermal blooming due to aerosols. *Appl Phys Lett*, 1975, 26 (11): 628 ~ 629.

[4] Sutton GW, Wong K. Light scattering by air heated from an aerosol due to pulsed irradiation. *J Appl Phys*, 1989, 65 (6): 2195 ~ 2189.

[5] Carslaw HS, Jaeger JC. Conduction of Heat in Solids (2nd edition). London: Oxford University Press, 1959. 247.

[6] 刘炎焱等. 光致气溶胶粒子加热对光传播的影响. 第二届全国激光技术青年科学会议. 北京. 1993, 6.2 ~ 7.

ANALYTIC THEORY OF SMALL-SCALE THERMAL BLOOMING INSTABILITIES

Shi Jiangjun

Institute of Southwest Physics,
P.O. Box 523-55, Chengdu 610003

ABSTRACT The linear analytic theory of small scale−size thermal blooming instabilities for a high energy laser propagating through a homogeneous medium is derived in paraxial scalar wave approximation and isobaric supposition. When we perform Fourier transforms in transversal coordinates and Laplace transforms in time and longitudinal coordinate, the fluctuations can be obtained in analytic form. In the real world the Fourier components of the fluctuations are written with the propagation kernal (or Green function) $K_k(z,t)$, after the inverting Laplace transforms are performed.

KEY WORDS thermal blooming, small scale−size instability, propagation kernel.

I. Introduction

Atmospheric propagation of a laser beam is restricted by instabilities due to thermal blooming. Small perturbations in intensity or in phase of the laser driving source will cause modulation of high-space frequency of laser beam intensity, thus leading to variation in medium refractivity due to absorption and other processes. These perturbations of the medium modulate the laser beam phase, intensifying the rate of laser beam perturbation relative to time and propagation distance.

Obviously, this interaction between laser and medium is nonlinear. A solution to this process requires equations from fluid mechanics on media as well as fluctuation equations of the combined light field. In addition, simulation solutions are carried out by using data encoding with a computer.

However, the field equations can considerably be simplified in the paraxial scalar wave approximation. In the isobaric approximation, the fluid-mechanical equations for the medium are very simple in form. In this status, researchers can very easily obtain the linear-perturbation equation set relating to light-intensity perturbation, phase perturbation, and medium-refractivity perturbation. In recent years, various methods of solutions were available for perturbation equation sets, such as, the Briggs' analytical method of approaching the solution [1], J. R. Morris' solutions on the standard Green function [2], and T. J. Karr's Laplace transform and inversion solution method [3]. Methods used in the article are similar to those used by Karr. Detailed derivations are presented in the article. Moreover, two kinds of equations are given to describe the propagation kernel $K_h(z,t)$ for growth in perturbation. These equations are used for reference by researchers on atmospheric propagation of high-powered lasers.

II. Theoretical Fundamentals

A laser field can be described by a complete set of Maxwell's equations. The laser propagates in the z-direction;

the propagation medium is nonmagnetic, with magnetoconductivity equal to magnetoconductivity in vacuo. The electrical charge in space and the conductive electric current in the medium are not taken into consideration. In addition, the dielectric constant of the medium is slow in time-space variation. Therefore, in the paraxial scalar wave approximation, the light field ε is

$$\varepsilon = E\exp\{i(\omega t - kz)\} \tag{1}$$

The light field envelope E=E(x,y,z,t,) satisfies the following equation

$$\nabla_{\perp}^2 E + 2ik\left(\frac{\partial}{\partial z} + \frac{\alpha_e}{2}\right)E + \left(\frac{\varepsilon}{\varepsilon_0} - 1\right)k^2 E = 0 \tag{2}$$

$k=2\Pi/\lambda$ is the number of laser waves and λ is the wavelength of the laser waves. α_e is the extinction coefficient, which is the summation of the absorption coefficient α_a and the scattering coefficient a_s; $\alpha_e=\alpha_a+\alpha_s$. Moreover, $\alpha_c=\mu_0\sigma c/n_0$; in the equation, μ_0, σ, and n_0 are, respectively, the magnetoconductivity, electroconductivity, and the background refractivity of the homogeneous medium, and c is the speed of light in vacuo.

The energy conversion time during which some of the laser beam energy is absorbed by the medium is much smaller than the propagation time of the laser beam; in atmospheric propagation, the energy conversion time is measured in microseconds and the propagation time is measured in seconds. In other words, the refractivity change of laser energy due to absorption by the medium occurs over a long time scale. Therefore, this process can be subject to the isobaric approximation. In the isobaric

approximation, the refractivity equation is

$$\frac{\partial n}{\partial t} + \mathbf{v} \cdot \nabla n = -\Gamma I + D\nabla^2 n \qquad (3)$$

In the equation, n = $\sqrt{\varepsilon}$ is the refractivity; ε is the dielectric constant of the medium; v is the fluid speed of the medium; and D is the mass diffusion coefficient of the medium. Caused by the unit laser intensity, the time variation rate Γ of refractivity is

$$\Gamma = c_b \alpha_e \qquad (4)$$

In the equation, $c_b = (\partial n/\partial \rho)_p/(c_p T)$. For a 20°C atmosphere, c_b is approximately equal to 8×10^{-4}cm^3/J $(\partial n/\partial \rho)_p$ is the Golstone-Dale constant; c_p is the isobaric specific heat of the medium; T is the background temperature of the medium; and I is the laser beam intensity

III. Linear Perturbation Equation

Assume I_0 and n_0 are, respectively, the laser intensity and refractivity of a medium in the absence of perturbation. Post-perturbation, laser intensity is I and medium refractivity is n. Let us also assume that the pre-perturbation field phase is ϕ_0, and that it is ϕ_1 post-perturbation, assuming that perturbation is very slight:

$$= I_0(1+F) \qquad (4.1)$$

$$\varphi = \varphi_0 - \varphi_1 \qquad (4.2)$$

$$n = n_0 + \Delta n \qquad (4.3)$$

Then the light field envelope $|E|=\sqrt{I}$ can be written as

$$E=E_0\sqrt{1+F}\exp\left(i(\varphi_0-\varphi_1)\right)\approx E_0\exp\left(i\varphi_0+\frac{F}{2}-i\varphi_1\right) \tag{5}$$

Let us introduce the variation of the relative refractivity

$$\mu=\frac{\Delta n}{n_0}\approx\frac{1}{2}\left(\frac{\varepsilon}{\varepsilon_0}-1\right)$$

Substitute Eq. (5) into Eq. (2), and substitute Eq. (4) into Eq. (3). By neglecting the higher-order perturbation terms (that is, adopting linear approximation),

$$\frac{\partial F}{\partial z}=-\frac{1}{k}\nabla_\perp^2\varphi_1 \tag{6.1}$$

$$\frac{\partial\varphi_1}{\partial z}=k\left(\mu+\frac{1}{4k^2}\nabla_\perp^2 F\right) \tag{6.2}$$

$$\frac{\partial\mu}{\partial t}+\mathbf{v}\cdot\nabla\mu=-\frac{\Gamma I_0}{n_0}F+D\nabla^2\mu \tag{7}$$

Eq. (6) can also be rewritten as

$$\frac{\partial^2 F}{\partial z^2}+\nabla_\perp^2\left(\mu+\frac{1}{4k^2}\nabla_\perp^2 F\right)=0 \tag{8}$$

Eqs. (7) and (8) are important equations in the analytical theory of thermal blooming small-scale instabilities. These equations present the variation rule of variable-refractivity propagation with propagation distance z and time t, for a medium, with the perturbation of laser intensity.

To solve for Eqs. (7) and (8), we should present the initial distribution μ (z=0) of perturbation F (z=0,t) for ϕ_1 (z=0,t) at the boundary (z=0).

IV. Perturbation Amount and Propagation Kernel

Execute a Fourier transform on Eqs. (7) and (8)

$$f_k = \iint_{-\infty}^{+\infty} f(x,y)\exp(ik\cdot r_{\_})\,dxdy/(2\pi)^2$$

In the equation, $k = k_x i + k_y j$, then the equation of the Fourier components of the perturbation quantity can be derived:

$$\frac{\partial^2 F_k}{\partial z^2} + a_k^2 F_k = k^2 \mu_k \tag{9}$$

$$\frac{\partial \mu_k}{\partial t} = -\Gamma^* F_k - Dk^2 \mu_k + iv\cdot k\mu_k \tag{10}$$

In the equations, the transverse-direction wave number k and a_k of the perturbation amount, and Γ^* are given below

$$\begin{aligned} k^2 &= k_x^2 + k_y^2 \\ a_k &= \frac{k^2}{2k} \\ \Gamma^* &= \Gamma I_0 / n_0 \end{aligned} \tag{11}$$

The corresponding initial condition and boundary condition are

$$\begin{aligned} F_k(t, z=0) &= F_k(0) \\ F_k'(t, z=0) &= F_k'(0) \\ \mu_k(z, t=0) &= \mu_k^0(z) \end{aligned} \tag{12}$$

Then, carry out a Laplace transform on z-σ and t-**v** in Eqs. (9) and (10), σ and **v** are, respectively, the conjugate variables of the Laplace transform. After manipulation, the expression formulas of the post-transform perturbation amounts are as follows:

$$\hat{\tilde{\mu}}_k = \frac{\sigma^2 + a_k^2}{v^*(\sigma^2 + a_k^2) + \Gamma^* k^2}\,\tilde{\mu}_k^0 - \frac{\Gamma^*(\sigma\hat{F}_k(0) + \hat{F}_k'(0))}{v^*(\sigma^2 + a_k^2) + \Gamma^* k^2} \tag{13}$$

$$\hat{\tilde{F}}_k = \frac{k^2}{v^*(\sigma^2 + a_k^2) + \Gamma^* k^2}\,\tilde{\mu}_k^0 + \left[1 - \frac{\Gamma^* k^2}{v^*(\sigma^2 + a_k^2) + \Gamma^* k^2}\right] \frac{\sigma\hat{F}_k(0) + \hat{F}_k'(0)}{\sigma^2 + a_k^2} \tag{14}$$

In the equations, $\nu^* = \nu - ik\cdot v + Dk^2$. When the convection velocity v and diffusion coefficient D are constant, the time factor $\exp(-Dk^2+ik\cdot v)$ is multiplied with the related quantities for obtaining the inverting transforms. We can see that the presence of diffusion has the function of restraining perturbation. However, the effect of the convection term is to change the transverse distribution of laser-intensity perturbation.

To carry out an inverting transform on Eqs. (13) and (14), let us introduce the following propagation kernels $\hat{\tilde{K}}_k, \hat{\tilde{L}}_k$, and $\hat{\tilde{K}}_k^0$:

$$\hat{\tilde{K}}_k = \hat{\tilde{K}}_k(\sigma, v) \equiv \frac{1}{v(\sigma^2+a_k^2)+\Gamma^* k^2} \tag{15}$$

$$\hat{\tilde{L}}_k = \hat{\tilde{L}}_k(\sigma, v) \equiv \frac{\sigma^2+a_k^2}{v(\sigma^2+a_k^2)+\Gamma^* k^2} \tag{16}$$

$$\tilde{K}_k^0 = K_k^0(\sigma) \equiv \frac{1}{\sigma^2+a_k^2} \tag{17}$$

Then the equations for perturbation expression equations (13) and (14) can be rewritten as:

$$\hat{\tilde{\mu}}_k = \hat{\tilde{L}}_k \tilde{\mu}_k^0 - \Gamma^* \hat{\tilde{K}}_k (\sigma \hat{F}_k(0) + \hat{F}_k'(0)) \tag{18}$$

$$\hat{\tilde{F}}_k = k^2 \hat{\tilde{K}}_k \tilde{\mu}_k^0 + (1-\Gamma^* k^2 \hat{\tilde{K}}_k)(\tilde{K}_k^{0\prime} \hat{F}_k(0) + \tilde{K}_k^0 \hat{F}_k'(0)) \tag{19}$$

In the equations, $K_k^{0\prime}$ is the Laplace transform of the $K_k^{0\prime}(z)$. Obviously,

$$\tilde{K}_k^{0\prime} = \sigma \tilde{K}_k^0 = \frac{\sigma}{\sigma^2+a_k^2} \tag{17'}$$

In the above-mentioned equations, those quantities with the symbol (^) indicate a Laplace transform with respect to time.

The quantities with the symbol '(~) indicate a Laplace transform of z. The quantities with superscript 0 indicate the initial value of time; the independent quantities containing 0 indicate the boundary value of the quantities. For example, $\tilde{\mu}_k^0$ indicates the quantity after the z-σ Laplace transform of the Fourier components for refractivity perturbation at the initial period. Besides, the quantities having an apostrophe at the superscript indicate the differential with respect to z. The quantities with ˙ indicate the differential of the quantity with respect to t.

By using the definitions (15) through (17) of the propagation kernel, we have the following relationships:

$$\begin{cases} \sigma\tilde{\tilde{K}}_k = \tilde{\tilde{K}}_k' \\ \tilde{\tilde{K}}_k' = -\Gamma^* k^2 \tilde{\tilde{K}}_k \tilde{K}_k^{0\prime} \\ \tilde{\tilde{K}}_k = -\Gamma^* k^2 \tilde{\tilde{K}}_k \tilde{K}_k^0 \\ \tilde{L}_k = -k^2\Gamma^* \int_0^t \tilde{K}_k(\tau)\, d\tau + 1 \end{cases} \tag{20}$$

among other relationships.

Let us carry out the inverting Laplace transform on z-σ in Eq. (18), and the inverting Laplace transform t-ν on Eq. (19); we can then obtain the solution of perturbations:

$$\mu_k(z,t) = L_k(z,t)\mu_k^0(z) - \Gamma^*[K_k'(z,t)F_k(0,t) + K_k(z,t)F_k'(0,t)] \tag{21}$$

$$F_k(z,t) = k^2 K_k(z,t)\mu_k^0(z) + K_k^{0\prime}(z)F_k(0,t) + K_k^0(z)F_k'(0,t) + \dot{K}_k'(z,t)F_k(0,t) + \dot{K}_k(z,t)F_k'(0,t) \tag{22}$$

We must note that in the two above-mentioned equations, in the

case of items containing two or more products independently multiplied by z, or items containing two or more products independently multiplied by t, these terms should be solved for with the convolution theorem according to the inverting Laplace transform. For example,

$$K_k'(z,t)F_k(0,t)=\int_0^t K_k(z,\tau)F_k(0,t-\tau)dt$$

$$K_k(z,t)\mu_k^0(z)=\int_0^z K_k(s,t)\mu_k^0(z-s)ds$$

among others (not written out here).

From the perturbation solution we know that there are three sources for stimulating instability: (1) intensity perturbation $F_k(0,t)$ of the laser transmission source (z=0); (2) phase perturbation $F_k'(0,t)$ of the laser transmission source (z=0); and (3) the initial perturbation $\mu_k(z,0)$ of refractivity in the medium. Only with the existence of any excitation source among them, can the growth in perturbation (after interaction between laser and medium) be given by using the propagation kernel $K_k(z,t)$, $L_k(z,t)$ and the corresponding post-differential quantity. We can see that it is vital to correctly present the expression equation of the propagation kernel $K_k(z,t)$.

V. Expression Equation for Propagation Kernel $K_k(z,t)$

From the definition of the propagation kernel $\tilde{K}_k(\sigma,\nu)$, σ-z is conducted with the inverting Laplace transform to obtain $\hat{K}_k(z,\nu)$. $\tilde{K}_k(\sigma,t)$ can be derived with the inverting Laplace transform on ν-t. There are the following results:

$$\hat{K}_k(z,v) = \frac{1}{v\alpha_k\beta}\sin(a_k\beta z) \tag{23}$$

$$\tilde{K}_k(\sigma,t) = \frac{1}{\sigma^2+a_k^2}\exp\left(-\frac{\Gamma^* k^2 t}{\sigma^2+a_k^2}\right) \tag{24}$$

In the equations,

$$\beta^2 = 1+\frac{v_0}{v}\ ,\quad v_0 = \frac{2k\Gamma^*}{a_k}$$

If the inverting Laplace transform of **v**-t is again carried out on $\hat{K}_k(z,v)$, or the inverting Laplace transform of σ-z is carried out on $\tilde{K}_k(\sigma,t)$, then the correct expression equation of the propagation kernel $K_k(z,t)$ can be obtained. In the inverting transform process, by utilizing the theorem of residues to solve for the integration of multi-pole point functions with the application of general integration equation of the inverting transform, and by utilizing the Lagrangian formula to complete the high-order differential of the multiplication product of two functions, thus the expression equation of $K_k(z,t)$ can be rigorously determined.

Beginning from Eq. (23), first $\hat{K}_k(z,v)$ is written in series form

$$\hat{K}_k(z,v) = \sum_{n=0}^{\infty}\frac{(-1)^n(a_k z)^{2n+1}}{(2n+1)!}\ \frac{1}{a_k}\ \frac{(v+v_0)^n}{v^{n+1}}$$

Then from the above-mentioned steps of the inverting transform, we obtain

$$K_k(z,t) = \sum_{n=0}^{\infty}\frac{(-1)^n(a_k z)^{2n+1}}{(2n+1)!}\ \frac{1}{a_k}\ \sum_{m=0}^{n}\frac{n!}{(n-m)!(m!)^2}\left(\frac{2k\Gamma^* t}{a_k}\right)^m \tag{25}$$

If beginning with Eq. (24), $K_k(z,t)$ can also be obtained.

First, $\tilde{K}_k(\sigma,t)$ is rewritten in the series form:

$$\tilde{K}_k(\sigma,t)=\sum_{n=0}^{\infty}\frac{(-1)^n(2k\Gamma^* a_k t)^n}{n!}\left(\frac{1}{\sigma^2+a_k^2}\right)^{n+1} \qquad (26)$$

There are (n+1) orders of pole points at the virtual axis $\sigma=\pm ia_k$ of the σ-complex plane. Complete the inverting transform with the above-mentioned steps, and the result is

$$K_k(z,t)=\sum_{m=0}^{\infty}\frac{(-1)^n(k\Gamma tz)^n}{(n!)^2}\frac{1}{a_k}S_n(a_k z) \qquad (26)$$

In the equation

$$S_n(a_k z)=\sum_{m=0}^{n}\frac{(-1)^m(n+m)!}{m!(n-m)!}\frac{1}{(2a_k z)^m}\frac{e^{ia_k z}+(-1)^{n+m+1}e^{-ia_k z}}{2(i)^{n+m+1}} \qquad (26')$$

Since there are different pathways of the inverting transform, there are quite different forms in $K_k(z,t)$ derived from Eqs. (25) and (26). However, since the field was begun from Eq. (15), the results are the same. If we let $K_k(z,t)=\sum_{n=0}^{\infty}K_k^{(n)}(z,t)$, we can obtain the following from the two equations mentioned above:

$$K_k^{(0)}=\frac{1}{a_k}\sin(a_k z)$$

$$K_k^{(1)}=\frac{k\Gamma^* t}{a_k^2}[a_k z\cos(a_k z)-\sin(a_k z)]$$

$$K_k^{(2)}=\frac{(k\Gamma^* t)^2}{a_k^3}\left[\frac{3}{4}\sin(a_k z)-\frac{3}{4}a_k z\cos(a_k z)-\frac{1}{4}(a_k z)^2\sin(a_k z)\right]$$

In the general situation, and in the situation of various parameters (a_k, z, t, Γ^*, k), by using the numerical dissolving method, we can prove that the $K_k(z,t)$ derived from Eq. (25) is identical to the $K_k(z,t)$ derived from Eq. (26). In $K_k(z,t)$, the

expression equation of $K_1^{(0)}$ not related to time is identical with the results of the inverting transform on the linear propagation kernel Eq. (17). This explains that both types of $K_1(z,t)$ expression equations are correct.

The first draft of the article was received on October 22, 1992; the revised final draft was received for publication on July 2, 1993.

REFERENCES

[1] Briggs RJ. Model of High Spatial Frequency Thermal Blooming Instabilities. UCID-21118, 1987.

[2] Morris JR. Standard Green's Function Derivation of the Thermal Blooming Compensation Instability Equation. UCID-21261-Rev1, 1987.

[3] Chambers DH, Karr TJ et al. Linear Theory of Thermal Blooming in Turbulence. UCID-102673, 1990.

[4] Karr TJ. Thermal Blooming Compensation Instabilities. UCID-21172, 1987.

ANISOPLANATISM IN ADAPTIVE OPTICS: EVALUATION IN TIME DOMAIN

Wang Yingjian

Anhui Institute of Optics and Fine Mechanics
Chinese Academy of Sciences,
Hefei 230031

ABSTRACT In this paper, anisoplanatism in adaptive optics and capability of phase derivative adaptive optics are analysed in time domain. The general formulas of residual phase structure function and Strehl ratio are obtained, which not only be used to discuss the anisoplanatism, but also can be used to analyse the other factors that degrade adaptive optics system performance, such as the mean wind velocity and the finite servo bandwidth of adaptive optics system. The results show that the capable scale of phase derivative adaptive optics are very narrow.

KEY WORDS adaptive optics, anisoplanatism, phase derivative.

I. Introduction

There has been much discussion on anisoplanatism in the eddy-current effect on laser atmospheric transmission compensated for with an adaptive-optics system [1,3]. A new method, the phase-gradient method, overcoming anisoplanatism, was presented in reference [3]. In the article, the time-domain analytical method is applied to further discuss the effect on compensation efficiency of an adaptive-optics system by anisoplanatism, mean wind field, and system bandwidth. Moreover,

the effect of the above-mentioned factors in phase compensation, and compensation under the phase gradient method is described from a unified standpoint of the time-domain (frequency-domain) transfer function of the adaptive-optics system. The article is the first to derive the general equations of the structure function of the residual phase with phase compensation and compensation under the phase gradient method. Next, the transfer function of the adaptive optical system in the phase gradient method is derived in the time domain of the Fourier transform time domain. Finally, the results are analyzed and discussed.

II. Strehl Ratio and Phase Structure Function

The result of compensating for the eddy-current effect in laser atmospheric transmission by an adaptive-optics system can be described with the Strehl ratio [4]:

$$St = \frac{4}{\pi D_0^2} \int d\vec{\rho} K(\vec{\rho}) \exp[-\frac{1}{2} D(\rho)] \qquad (1)$$

In the equation

$$K(\vec{\rho}) = \begin{cases} \frac{2}{\pi} [\arccos(\frac{|\vec{\rho}|}{D_0}) - \frac{|\vec{\rho}|}{D_0} \sqrt{1-(\frac{|\vec{\rho}|}{D_0})^2} & , (|\vec{\rho}| \leq D_0) \\ 0 & , (|\vec{\rho}| > D_0) \end{cases} \qquad (2)$$

is the modulated transfer function of the laser transmission system; D_0 is the transmission aperture; and $\vec{\rho}$ is the coordinate difference of the deformation mirror surface in the adaptive-optics system.

$$D(\vec{\rho}) = D_s(\vec{\rho}) + D_\chi(\vec{\rho}) \tag{3}$$

D_s and D_χ are, respectively, the structure functions of the fluctuating phase and oscillation amplitude. We do not discuss here the effect on fluctuating oscillation amplitude. The phase structure function is given by

$$D_s(\vec{\rho}) = \langle [\Delta\Phi(r_1, t) - \Delta\Phi(r_2, t)]^2 \rangle \tag{4}$$

$\Delta\Phi(r,t)$ is the residual phase of the transmitted light beam; $\langle\ \rangle$ indicates the statistical mean. In the approximate conditions of geometric optics, the anomaly phase generated by atmospheric transmission of a laser through eddy currents is given by the following:

$$\Delta\Phi_T(r,t) = k\int_0^h dz n[r + (\vec{\theta} z + v_0)t, z] \tag{5}$$

$k = 2\pi/\lambda$; is the number of laser waves; n is the fluctuating refractivity; h is the transmission distance; $\vec{\theta}$ is the angular velocity of target motion or the wind speed vector in the atmosphere; and v_0 is the mean wind velocity in the atmosphere. As is well known, there is a time lag in the adaptive optical system. Let us assume that the time lag is Δt, that the phase relationship between the beacon light and the main laser with compensation of phase is given by

$$\Phi_B(r, t+\Delta t) = \Phi_T(r,t) \tag{6}$$

Φ_B、Φ_T indicate, respectively, the phase of the beacon light and the phase of the main laser. Therefore, during the actual phase compensation there is a residual phase $\Delta\Phi$

$$\Delta\Phi(r, t+\Delta t) = \Phi_T(r, t+\Delta t) - \Phi_B(r, t+\Delta t) = \Phi_T(r, t+\Delta t) - \Phi_T(r,t) \tag{7}$$

Thus we know that during the phase compensation, the structure function of the residual phase is

$$D_r(\vec{\rho},t)=k^2\int_0^h dz_1\int_0^h dz_2\langle[n(r_1,t+\Delta t,z_1)-n(r_2,t+\Delta t,z_1)-n(r_1,t,z_1)+n(r_2,t,z_1)]\times[n(r_1,t+\Delta t,z_2)-n(r_2,t+\Delta t,z_2)-n(r_1,t,z_2)+n(r_2,t,z_2)]\rangle \quad (8)$$

Let $z=z_1-z_2$; with further derivation, we obtain

$$D_r(\vec{\rho},t)=k^2\int_0^h dz_1\int_{-h}^h dz[-2D_n(0,z)+2D_n(|\vec{\rho}|,z)+2D_n(|\vec{\rho}|,z)-D_n(|\vec{\rho}+\vec{\rho}_1|,z)-D_n(|\vec{\rho}-\vec{\rho}_1|,z)] \quad (9)$$

In the equation, $\vec{\rho}_1=(\vec{\theta}z_1+v_0)\Delta t$, $D_n(|\vec{\rho}|,z)=C_n^2(\frac{z_1+z_2}{2})(|\vec{\rho}|^2+z^2)^{1/3}$ is the structure function of the perturbation refractivity; is the structure constant of the perturbation refractivity. Since in the general situation the integration limit of $\Delta z\gg|\vec{\rho}|$, dz can be extended to $(-\infty,\infty)$, thus Eq. (9) becomes

$$D_r(\vec{\rho},\Delta t)=2.91k^2\int_0^h dz_1 C_n^2(z_1)[2|\vec{\rho}|^{5/3}-|\vec{\rho}+\vec{\rho}_1|^{5/3}-|\vec{\rho}-\vec{\rho}_1|^{5/3}+2|\vec{\rho}_1|^{5/3}] \quad (10)$$

In the above equation, $I_1(\frac{1}{3})=\int_{-\infty}^{\infty}[(1+x^2)^{1/3}+(x^2)^{1/3}]dx\approx 2.91.$ is applied.

If the phase gradient compensation is applied, we have

$$\Phi_B(r,t+\Delta t)=\Phi_B(t)+\frac{\partial\Phi_B(t)}{\partial t}\Delta t=\Phi_B(t)+\frac{\Phi_B(t+\Delta t)-\Phi_B(t-\Delta t)}{2\Delta t}\Delta t \quad (11)$$

From Eqs. (6) and (5), we can obtain

$$\Phi_B(r,t+\Delta t)=2\Phi_T(r,t)-\Phi_T(r,t-\Delta t) \quad (12)$$

$$\Delta\Phi(r,t+\Delta t)=k\int_0^h dz[\,n(r,t+\Delta t,z)-2n(r,t,z)+n(r,t-\Delta t,z)\,] \qquad (13)$$

By using a method similar to that mentioned above, we can obtain the result that in the compensation situation of the phase gradient, the structure function $D_{s_1}(\vec{\rho},\Delta t)$ for the residual phase is

$$D_{s_1}(\vec{\rho},\Delta t)=2.91k^2\int_0^h dz_1 C_n^2(z_1)[\,6|\vec{\rho}|^{5/3}-4|\vec{\rho}+\vec{\rho}_1|^{5/3}-4|\vec{\rho}-\vec{\rho}_1|^{5/3}$$
$$+|\vec{\rho}+2\vec{\rho}_1|^{5/3}+|\vec{\rho}-2\vec{\rho}_1|^{5/3}+8|\vec{\rho}_1|^{5/3}-2|2\vec{\rho}_1|^{5/3}] \qquad (14)$$

In the following, we apply the time-domain Fourier-transform method (as described in reference [2]) for processing, that is,

$$\Phi_T(r,f)=\int dt\,\Phi_T(r,t)\exp[-2\pi i f t] \qquad (15)$$

f is the conjugate variable of the Fourier transform for time t. $\Phi_B(r,f)$ can be used to describe the following relationship:

$$\Phi_B(r,f)=H(f)\Phi_T(r,f) \qquad (16)$$

H(f) is the Fourier transform of the time-domain transfer function in the adaptive-optics system. With processing similar to that mentioned above, the general equation of the residual-phase structure function [2] can be obtained:

$$D_s(\vec{\rho})=2.91k^2\iiint df\,dt\,dz_1\,|1-H(f)|^2\exp[-2\pi i f t]$$
$$\cdot C_n^2(z_1)[\,\frac{1}{2}|\vec{\rho}+\vec{\rho}_1|^{5/3}+\frac{1}{2}|\vec{\rho}-\vec{\rho}_1|^{5/3}-|\vec{\rho}_1|^{5/3}] \qquad (17)$$

In the phase compensation situation, from Eq. (6) we know

$$H(f)=\exp[-2\pi i f\Delta t] \qquad (18)$$

Let us substitute Eq. (18) into Eq. (17) and we can obtain Eq.

(10). With respect to compensation under the phase gradient method, from Eq. (12) we can obtain

$$\Phi_{s_1}(r,f)=2H(f)\Phi_T(r,f)-H^2(f)\Phi_T(r,f)=H_1(r,f)$$

that is, during compensation under the phase gradient method, the Fourier transform of the time-domain transfer function in the adaptive-optics system is

$$H_1(f)=H(f)[2-H(f)] \qquad (19)$$

Thus, let us substitute Eqs. (18) and (19) into Eq. (17), and we can very easily obtain results similar to that in Eq. (14).

III. Discussion

From the foregoing analysis we know that Eq. (17) is the general equation describing the structure function of the residual phase for the time-domain error in the adaptive-optics system. More detailed discussion [2] was conducted on the effect of anisoplanatism in the situation of response bandwidth and phase compensation in the adaptive-optics system. Here we discuss mainly the difference of the effect by the atmospheric mean wind field and anisoplanatism in phase compensation and compensation under the phase gradient method. Furthermore, we can know the adaptation range in the phase gradient method.

3.1. Effect of Mean Wind Field

When $\vec{\theta}=0$, $\vec{\rho}_1=v_0\Delta t$, since the deviation of the transmission channel of the main laser and the beacon light due to the mean wind field will bring errors into phase compensation, and thus

reduce the Strehl ratio, we first analyze two extreme cases.

When $|\vec{\rho}_1/r_0| \ll D_0/r_0$ from Eqs. (1), (10), and (14), we obtain the Strehl ratios St and St_1 of laser atmospheric transmission of phase compensation and compensation under the phase gradient method, respectively, as:

$$St = \exp[-6.88|\frac{\vec{\rho}_1}{r_0}|^{5/3}]$$
$$St_1 = \exp[-5.676|\frac{\vec{\rho}_1}{r_0}|^{5/3}] \quad (20)$$

In the equations, r_0 is the transverse-direction coherent length. From Eq. (20), then we can see that compensation under the phase gradient method is better than phase compensation. We define it as follows: when the Strehl ratio is reduced to 1/e,

$|\vec{\rho}_1|$ is the isoplanatic length. Then in the situation of phase compensation and compensation under the phase gradient method, the isoplanatic lengths ρ_0 and ρ_{01} are, respectively:

$$\rho_0 = 0.3144 r_0$$
$$\rho_{01} = 0.3528 r_0 \quad (21)$$

We know that the isoplanatic length with compensation under the phase gradient method is 1.122 times the isoplanatic length during phase compensation.

When $|\vec{\rho}_1/r_0| \gg D_0/r_0$, that is the case of entirely different optical paths for the beacon light and the main laser, then we have

$$D_t(\vec{\rho}) = 2 \times 6.88|\frac{\vec{\rho}}{r_0}|^{5/3}$$
$$D_{t_1}(\vec{\rho}) = 6 \times 6.88|\frac{\vec{\rho}}{r_0}|^{5/3} \quad (22)$$

However, the phase structure function without phase compensation

is $6.88\,|\vec{\rho}/r_0|^{5/3}$, then we can see that the phase compensation is not worse than in the absence of compensation, and compensation under the phase gradient method is even worse than phase compensation. In other words, applying an unrelated phase for compensation in the present transmission situation is even worse than the absence of compensation.

For the general situation, from Eqs. (1), (10), and (14) we can obtain

$$
\begin{aligned}
St &= \frac{4}{\pi D_0^2}\int d\vec{\rho}\,k(\vec{\rho})\exp\{-3.44[2|\frac{\vec{\rho}}{r_0}|^{5/3}-|\frac{\vec{\rho}+\vec{\rho}_1}{r_0}|^{5/3}-|\frac{\vec{\rho}-\vec{\rho}_1}{r_0}|^{5/3}+2|\frac{\vec{\rho}_1}{r_0}|^{5/3}]\} \\
St_1 &= \frac{4}{\pi D_0^2}\int d\vec{\rho}\,k(\vec{\rho})\exp\{-3.44[6|\frac{\vec{\rho}}{r_0}|^{5/3}-4|\frac{\vec{\rho}+\vec{\rho}_1}{r_0}|^{5/3}-4|\frac{\vec{\rho}-\vec{\rho}_1}{r_0}|^{5/3} \\
&\quad +|\frac{\vec{\rho}+2\vec{\rho}_1}{r_0}|^{5/3}+|\frac{\vec{\rho}-2\vec{\rho}_1}{r_0}|^{5/3}+1.65|\frac{\vec{\rho}_1}{r_0}|^{5/3}]\}
\end{aligned}
\tag{23}
$$

Fig. 1 shows the comparison of the Strehl ratio for atmospheric transmission of a laser in the presence of eddy current during phase compensation and with compensation under the phase gradient method in different situations of $|\vec{\rho}_1/r_0|$: a, b, c are the results of phase compensation ; d, e, f are the results of compensation under the phase gradient method. a, d : $|\vec{\rho}_1/r_0|=0.1$; b, e : $|\vec{\rho}_1/r_0|=0.31$; c, f : $|\vec{\rho}_1/r_0|=1.0$. From Fig. 1, we can see that the results of $|\vec{\rho}_1/r_0| \ll D_0/r_0$ and $|\vec{\rho}_1/r_0| \gg D_0/r_0$ are consistent with the results in the above-mentioned analyses. For different $|\vec{\rho}_1/r_0|$, there is a critical D_0/r_0. When D_0/r_0 is lower than the critical value, in the case of compensation under the phase gradient method the decrease in the Strehl ratio with increase in

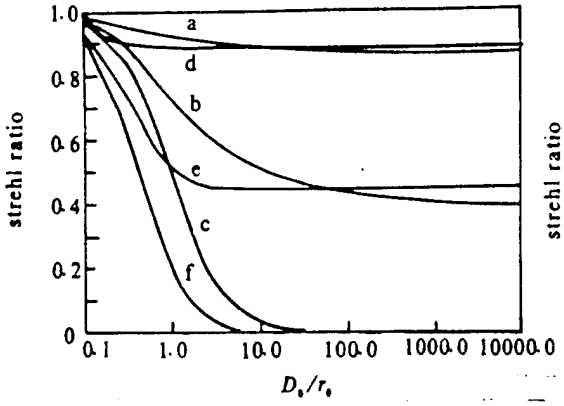

Fig. 1 Strehl ratio *vs* D_0/r_0 at different $|\vec{\rho}_1/r_0|$ with phase and phase derivative compensation

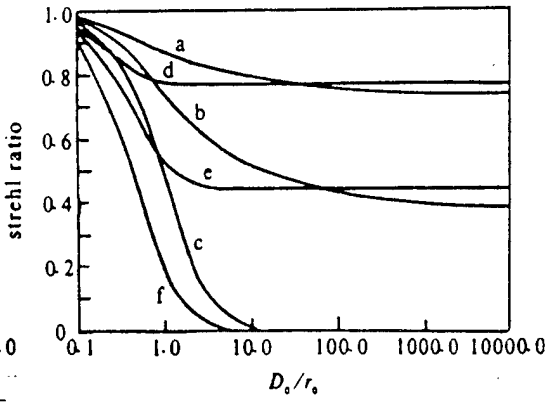

Fig. 2 Strehl ratio *vs* D_0/r_0 at different θ/θ_0 with phase and phase derivative compensation

D_0/r_0 is more rapid than that under phase compensation, and it is smaller than the Strehl ratio in phase compensation. When D_0/r_0 is greater than the critical value, in compensation under the phase gradient method the Strehl ratio more rapidly approaches the limiting value; this is the result shown in Eq. (20). Then compensation under the phase gradient is better than phase compensation. Moreover, with increase in $|\vec{\rho}_1/r_0|$, the critical value of D_0/r_0 is higher. The physical reason is as follows: on the one hand, when $|\vec{\rho}_1/r_0|$ is a constant, with increase in D_0/r_0, the residual phase is greater in phase compensation and in compensation under the phase gradient method; thus, the Strehl ratio decreases with increase in D_0/r_0. On the other hand, when D_0/r_0 is smaller, with r_0 held constant, $|\vec{\rho}_1/r_0|$ is greater, and $|\vec{\rho}_1/D_0|$ is also greater. The phase relationship between the beacon light and the main laser is more deteriorated, thus not only is the residual phase difference greater under phase

compensation, and the correlated phase difference in compensation under the phase gradient method is also greater. Thus, the Strehl ratio decreases with increase in $|\vec{\rho}_1|/r_0|$. This also causes compensation under the phase gradient method to be worse than phase compensation.

3.2. Anisoplanatism

When $\nu_0=0$ and $\vec{\theta}\neq 0$, there is an included angle $\theta=|\vec{\theta}|\Delta t$ between the beacon light and the main laser. This also will engender an error in the phase compensation. Similarly, we first analyze two extreme cases.

When $\theta \ll D/h$, from Eqs. (1), (10), and (14), we obtain the result that the Strehl ratios St and St_1 are, respectively, expressed in Eq. (24) and in phase compensation under the phase gradient method

$$\begin{aligned} St &= \exp[-(\frac{\theta}{\theta_0})^{5/3}] \\ St_1 &= \exp[-0.825(\frac{\theta}{\theta_0})^{5/3}] \end{aligned} \tag{24}$$

Here, Θ_0 is the isoplanatic angle [2] in phase compensation

$$\theta_0=[2.91k^2\int_0^h dz z^{5/3}C_n^2(z)]^{-3/5} \tag{25}$$

Similarly, we define that Θ is the isoplanatic angle Θ_{01} when the Strehl ratio decreases to 1/e in compensation under the phase gradient method, then we have

$$\theta_{01}=1.122\theta_0$$

We can see that the isoplanatic angle in compensation under the

phase gradient method is 1.122 times the isoplanatic angle under phase compensation. However, when $\theta \gg D/h$, there is the similar result as in Eq. (20). In other words, the phase compensation is worse than in the absence of compensation, and compensation under the phase gradient method is even worse than phase compensation.

In the general situation, from Eq. (1), (10), and (14), we calculate the Strehl ratio in phase compensation and in compensation under the phase gradient method for different Θ/Θ_0 values. The results are shown in Fig. 2a, b, c, as the results in phase compensation; d, e, and f are the results in compensation under the phase gradient method. a、d : $\theta/\theta_0=0.5$; b、e : $\theta/\theta_0=1.0$; c、f : $\theta/\theta_0=5.0$. The calculation condition is that there is the horizontal homogeneous atmosphere. With respect to an inhomogeneous atmosphere, the results do not intrinsically differ. From Fig. 2, the fundamental result is similar to the effect of the main wind field.

From the foregoing analysis, only in the case when there are smaller $|\vec{\rho}_1/r_0|$ and Θ/Θ_0, and D_0/r_0 is greater, the compensation under the phase gradient method then be better than phase compensation. From Figs. 1 and 2, we see that when $|\vec{\rho}_1/r_0|$ = 0.1 and 0.31, as the phase gradient method is better than the phase method that the critical values of D_0/r_0 are, respectively, 20 and 55. When Θ/Θ_0=0.5 and 1.0, the critical values D_0/r_0 are, respectively, 30 and 70. In the case of even smaller Θ/Θ_0 and $|\vec{\rho}_1/r_0|$, there is very slight differences in the effect on compensation under the phase gradient method and on

phase compensation. With the greater $|\vec{\rho}_1/r_0|$ and Θ/Θ_0, in the effective range the phase gradient method does not have superiority. Even when D_0/r_0 is much greater than $|\vec{\rho}_1/r_0|$, or D_0/r_0 is much greater than Θ/Θ_0, the isoplanatic length and the isoplanatic angle in compensation under the phase gradient method are only 1.122 times the isoplanatic length and the isoplanatic angle in phase compensation.

4. Conclusions

By using the time domain analytic method, the author and his colleagues obtained the general equations, Eqs. (1) and (17), of the residual phase structure function and the Strehl ratio in the effect of an adaptive-optics system during anisoplanatism, mean wind field, and the system finite bandwidth. The results are consistent with those in reference [2]. The effect on mean wind field and anisoplanatism in phase compensation and in compensation under the phase gradient method are emphasized in the analysis. As revealed in the results, when $|\vec{\theta}h + v_0|\Delta t \ll D_0$, the isoplanatic region compensated under the phase gradient method is only 1.122 times the isoplanatic region compensation in phase compensation. However, when $|\vec{\theta}h + v_0|\Delta t$, the phase compensation is worse than the absence of compensation, and the compensation under the phase gradient method is even worse than phase compensation. For general cases, even as the Strehl ratio in compensation under the phase gradient method is several times greater than that of phase compensation, but then the Strehl

ratio is considerably lower than the actual requirement. We can see that the compensation of the eddy-current effect in laser atmospheric transmission is not very effective under the phase gradient method. Even to a certain extent, compensation under the phase gradient method is better than phase compensation, but the effective range is very narrow, and the extent of improvement is also very limited. Moreover, there will be greater complexity in the adaptive-optics system, and higher computation volume in the wavefront processing.

The author expresses his gratitude to researcher Song Zhengfang for valuable discussions during the writing of this paper.

The first draft was received on February 15, 1993; the final revised draft was received for publication on June 5, 1993.

REFERENCES

[1] Fried DL. Anisoplanatism in Adaptive Optics. *J O S A*, 1982, 72: 52 ~ 61.

[2] Tyler GA. Turbulence Induced Adaptive Optics Performance Degradation: Evaluation in the Time Domain. *SPIE Proc*, 1983, 410: 179 ~ 188.

[3] 冯岳忠，龚知本，宋正方. 自适应光学中的非等晕性. 强激光与粒子束, 1991, 3(1): 65 ~ 72.

[4] 宋正方. 强湍流区的自适应光学适用性. 强激光与粒子束, 1992, 4(3): 405 ~ 410.

NEAR-SITE VERIFICATION OF TESTING POWER OF GROUND-BASED HIGH-POWERED LASER

Li Bin and Du Xiangwan
Beijing Institute of Applied Physics
and Computational Mathematics
P.O. Box 8009, Beijing 100088

ABSTRACT The verification of testing power of ground-based high power laser is an important physical problem in arms control. In this paper we propose a scheme to measure the scattering light of laser beam in atmosphere by multi-detector. The optimal detective parameters are calculated and several algorisms to evaluate the laser power are studied.
KEY WORDS verification of laser power, arms control, scattering by aerosol.

I. Introduction

The firing level of high-powered laser weapons is directly related to the power of laser devices. To prevent further development of high-powered laser weaponry from becoming a threat to space targets and to inhibit the arms race in space, scientists proposed the concept of limiting the development of laser weapons by limiting the power at which lasers can be tested in the atmosphere [1]. This requires an appropriate method of evaluating laser power in testing. Although it is convenient and effective to directly measure laser power in laboratories, such evaluation schemes may be difficult to accept by those under

inspection. Therefore, a method should be found to estimate laser power from a certain distance. T. H. Braid [2,3] proposed a scheme to estimate laser power by measuring the aerosol scattering light in the atmosphere. Under the assumption that scattering is isotropic, Braid et al. also proved that the scattering light for a laser beam capable of attacking targets in outer space is very intense. There is still a very high signal-to-noise ratio detectable beyond distances of 1km. Therefore, this evaluation scheme is feasible.

Actually, the aerosol scattering of laser beams in the infrared band is anisotropic; the difference of light intensity at different scattering angles can be assigned in three orders of magnitude. Since the direction of the test laser beam can be randomly varied within a certain range, the scattering angle also changes from laser beam to sensor. Therefore, the power of scattered light received by the sensor is also variable so there will be great error in estimating the laser power based on this approach. To reduce the estimation error engendered by uncertain laser beam direction to meet the requirements of evaluation, the authors proposed a scheme for detecting scattered light with multiple sensors.

During target practice tests with lasers, the target can also be used to evaluate laser power from the diffused reflected laser light. The evaluation method discussed in the paper does not include this case.

II. Fundamental Principle

Usually, the atmospheric transmission and the comprehensive demonstration tests of laser weapons are selected at sites with good meteorological conditions, conducted on sunny days with higher visibility. Here, laser beam transmission over thousands of meters will not suffer from obvious attenuation. Moreover, the function of multiple scattering can also be neglected. The sensors used to monitor laser scattered light is in the order of magnitude of approximately, in distance from the laser beam, in the range of kilometers, much greater than the laser beam range. Under these conditions the power of laser scattered light received at the sensors is:

$$P_D = P \int \beta(r,\theta) \cos\alpha S dl / D^2 \qquad (1)$$

In the equation, P is the laser beam power. $\beta(r,\Theta)$ is scattering coefficient of the volumetric angle at point r with scattering angle Θa. α is the incident angle of the scattered light at the sensor. S is the sensor area. l is the distance along the light beam from any point r to the light source. D is the distance from point r to the sensor.

Within the range of thousands of meters near the ground, the aerosol particle size distribution is almost constant, with concentration gradually decreasing with height h. Therefore, the scattering coefficient of the volumetric angle can be expressed as:

$$\beta(r,\theta) = \beta(\theta) \exp\left(-\frac{h}{H_r}\right) \qquad (2)$$

In the equation $\beta(\Theta)$ is the scattering coefficient of the volumetric angle for the aerosol on ground level; and H_p is the datum of the aerosol [4,5]

$$H_p \approx 1.4\text{km} \tag{3}$$

Hence,

$$P_D = PS\int \beta(\theta)\exp\left(-\frac{h}{H_p}\right)\frac{\cos\alpha}{D^2}\,dl \tag{4}$$

If the aerosol particle size distribution in the laser beam direction as well as the sensor position and direction are not changed, then power P_D of the scattered light detected is proportional to laser power P. By using a laser with known power as a scale, laser power P can be estimated based on scattered light. The uncertainty of laser beam direction will cause errors under this estimation method. The estimated related error is correlated with the shape of the scattering coefficient $\beta(\Theta\text{theta})$ of the volumetric angle. Fig. 1 shows three typical scattering-angle curves on sunny days [6]. From Fig. 1, we can see that this scattering is anisotropic.

III. Evaluation Scheme

Along the circular circumference at a distance x_0 from the light source to be evaluated, several sensors are placed at equal spacing along the circumference. And each sensor is facing the direction of the light source. The elevation angle of the sensor is γ. Its longitudinal-direction opening angle is ω; its transverse-direction opening angle is 180°. So, the angle of field-of-view is $\omega \times 180^\circ$.

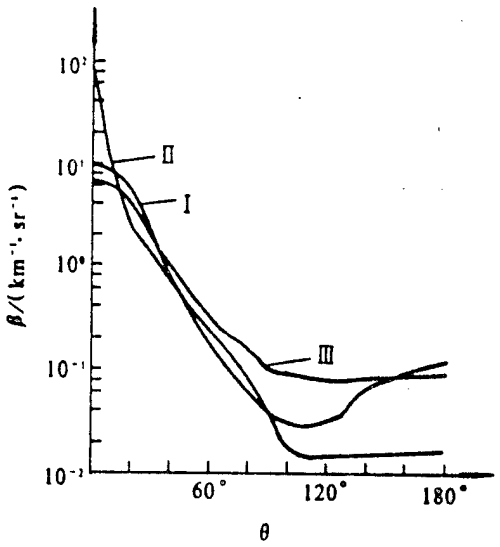

Fig. 1 Angular scattering functions of water haze with Young particle-size distribution function (ρ_{m_1} = 0.05μm, ρ_{m_2} = 5.00μm, power exponent β_r)

Curves 1: β_r = 3, λ = 10.6μm

2: β_r = 3, λ = 1.15μm

3: β_r = 4, λ = 10.6μm

Let us assume that the position of the laser light source is at the origin of coordinates. The connected line between the light source and any sensor i is the x-axis. Then the coordinates of sensor i are $(x_0, 0, 0)$. Assume that the pole angles of the laser beam are (Θ_m, ϕ_m), then the coordinates of any point on the laser beam are $(l\sin\theta_m\cos\varphi_m,\ l\sin\theta_m\sin\varphi_m,\ l\cos\theta_m)$. The height of point r is

$$h = l\cos\theta_m \tag{5}$$

After calculations, the distance from point r to the sensor i is

$$D = (x_0^2 + l^2 - 2x_0 l\sin\theta_m\cos\varphi_m)^{1/2} \tag{6}$$

The scattered angle from point r scattering to sensor i is

$$\cos\theta = \frac{x_0\sin\theta_m\sin\varphi_m - l}{(x_0^2 + l^2 - 2x_0\sin\theta_m\cos\varphi_m)^{1/2}} \tag{7}$$

The angle of incidence of the scattered light onto the sensor i is

$$\cos\alpha = \frac{\cos\gamma(x_0 - l\sin\theta_m\cos\varphi_m) + l\cos\theta_m\sin\gamma}{(x_0^2 + l^2 - 2x_0 l\sin\theta_m\cos\varphi_m)^{1/2}} \tag{8}$$

Since there is a certain limitation at the longitudinal-direction for the field-of-view angle for the sensor, points of too high and too low on the laser beam are situated outside of the field-of-view angle, therefore light passing through these points cannot reach the sensor. By calculation, we know that the lowest point capable of reaching the sensor is

$$l_{min} = \frac{x_0}{\cos\theta_m + \sin\theta_m\cos\varphi_m \operatorname{ctg}(\gamma - \frac{\omega}{2})} \tag{9}$$

the highest point capable of reaching the sensor is

$$l_{max} = \begin{cases} \infty \text{ , 当} \cos\theta_m + \sin\theta_m\cos\varphi_m \operatorname{ctg}(\gamma + \frac{\omega}{2}) \leqslant 0 \\ \dfrac{x_0}{\cos\theta_m + \sin\theta_m\cos\varphi_m \operatorname{ctg}(\gamma + \frac{\omega}{2})} \text{ , and others} \end{cases} \tag{10}$$

Let us substitute Eqs. (3), (5), (6), (7), (8), (9), and (10) in Eq. (4) and we can calculate that the scattered light power, which can be received by the sensor i is

$$P_{D_i} = PS\int_{l_{min}}^{l_{max}} \beta(\theta)\exp(-\frac{h}{H_p}) \frac{\cos\alpha}{D^2}\, dl \tag{11}$$

A calculation was made by the authors by using an example of a 1km distance between the sensor and the laser source, taking

$$x_0 = 1\text{km} \tag{12}$$

V. Power Estimation Method

Based on Eq. (11), we can determine the scattered light power measured for each sensor. When the laser beam direction is upward, the scattered light power measured by each sensor is the same. When the laser beam direction changes, generally speaking there are different scattered light power values received at each sensor. The authors tried three algorithms to average the scattered light power received by each sensor. Then the average scattered light power is used to estimate the laser beam power.

(a) Arithmetic mean

$$\overline{P}_D = \frac{1}{n}\left(\sum_{i}^{n} P_{D,i}\right) \tag{13}$$

In the equation, n is the number of sensors. $P_{D,i}$ is derived from Eq. (11).

(b) Post-selection average

Remove the maximum and minimum power of the scattered light just measured, the arithmetic mean is found from the remaining (n-2) data:

$$\overline{P}_D = \frac{1}{n-2}\left[\sum_{i=1}^{n} P_{D,i} - \max(P_{D,i}) - \min(P_{D,i})\right], \quad n \geq 3 \tag{14}$$

(c) Weighted average

A certain order of power of $P_{D,i}$ is used as the weighting factor, therefore this can also be called the power-based average:

$$\overline{P}_D = \left[\frac{1}{n}\sum_{i=1}^{n} P_{D,i}^{w}\right]^{\frac{1}{w}} \tag{15}$$

In the equation w is a parameter that can be used to calculate an

optimal value.

After not a long period (less than 1h) before and after the laser tests in the atmosphere for the evaluation, a laser beam with known power P_0 is vertically emitted from the laser light source in order to scale the system. Now, the power $P_{D,0}$ received at each sensor is the same. The following equation can be used to estimate laser power.

$$P' = P_0 \frac{\overline{P_D}}{P_{D,0}} \tag{16}$$

In the equation, $\overline{P_D}$ is given by Eqs. (13), (14), or (15). The estimated laser power P' may not be definitely equal to the actual laser power P. The estimated relative error is

$$\varepsilon = \frac{P' - P}{P} \tag{17}$$

The estimated errors from different laser beam directions (θ_m, φ_m) are not the same. By changing the direction γ and field-of-view angle of the sensor, the error values will also change. In other words, ε is a function of $\theta_m, \varphi_m, \gamma$

$$\varepsilon = \varepsilon(\theta_m, \varphi_m; \gamma, \omega) \tag{18}$$

We assume that the included angle between the laser beam and the vertical direction does not exceed 60^0 because the distance of a laser beam passing through the atmosphere is Θ_m exceeds 60^0. This makes it disadvantageous for a laser beam to pass through the atmosphere. The authors request that the estimated errors ε of all possible laser beam directions and powers should be as

small as possible. Therefore, the author defined the mean error for the laser beam direction (Θ_m, ϕ_m).

$$\bar{\varepsilon}(\gamma,\omega)=\left[\frac{1}{60^\circ\times 360^\circ}\int_0^{60^\circ} d\theta_m \int_0^{360^\circ} d\varphi_m \varepsilon^2(\theta_m,\varphi_m;\gamma,\omega)\right]^{1/2} \qquad (19)$$

The minimum value is to be sought for the mean error $\bar{\varepsilon}$:

$$\min[\bar{\varepsilon}(\gamma,\omega)] \qquad (20)$$

We can obtain the optimal detection parameters γ_0 and ω_0 as well as the diameter w_0 in Eq. (15).

V. Results of Calculations

For scattering-curve angle I, three methods (a), (b), and (c) are used to estimate the power to separately derive three sets of the optimal detection parameter γ_0 and ω_0, as well as the parameter w_0 in Eq. (15) (refer to Table 1).

Fig. 2 shows the relationship of the variable estimation error ε with ϕ_m when using method (a) of the arithmetic mean for eight sensors, when $\omega=0.001^\circ$, $\alpha=63.5^\circ$, $\Theta_m=60^\circ$, and laser direction varying from 0° to 360°. Fig. 3 shows the relationship between the mean error and the detection direction γ, while adopting the averaging method (a) with eight detectors and $\omega=0.001^\circ$. We can see that the optimal detection direction $\gamma_0=63.5^\circ$. Fig. 4 shows the relationship between the mean error $\bar{\varepsilon}$ and the field-of-view angle when the method of averages (a) is used with eight

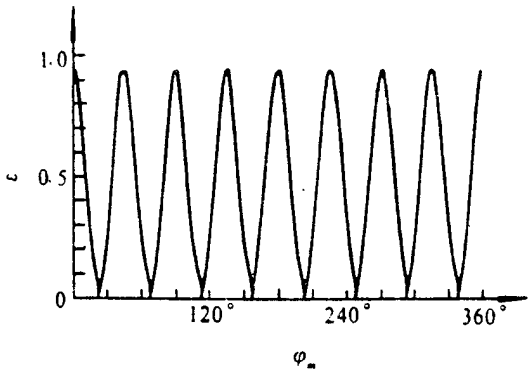

Fig. 2 Error varies as the angle of laser beam φ_n

sensors and $\gamma=63.5^{\circ}$. We can see that the mean error is at a minimum when the field-of-view angle ω approaches 0. Actually, the field-of-view angle cannot be equal to 0. Only with a smaller field-of-view angle, to be given, such as $\omega=0.001^{\circ}$ or $\omega=1^{\circ}$, does the mean error still approach the minimum values.

After testing the change of laser wavelength, or the change in the aerosol particle size distribution with climate, the shape of the scattering-angle curve will also changed. However, the direction and angle of the field of view of the sensor are set in advance so these cannot be changed. The authors still applied the angle scattering curve I to attain three sets of detection parameters in order to calculate the mean errors of the scattering-angle curves II, and III. By adopting three power estimation methods and three scattering-angle curves, different mean errors and maximum errors are obtained for different sensors. These values are listed in Table 1.

VI. Conclusions

From Table 1, we can see that the mean error can be smaller than 20% and the maximum error can be smaller than 50% due to

Table 1 Mean Errors and Maximum Errors

number of detectors n	(a) arithmetic average $\gamma=63.5^\circ$, $\omega=0.001^\circ$		(b) average after choise $\gamma=65.0^\circ$, $\omega=0.001^\circ$		(c) weighted average $w=0.441$, $\gamma=40.9^\circ$, $\omega=0.001^\circ$	
	$\bar{\varepsilon}$	$\max(\varepsilon)$	$\bar{\varepsilon}$	$\max(\varepsilon)$	$\bar{\varepsilon}$	$\max(\varepsilon)$
Errors for Angular Scattering Curve I						
1	1.026	10.71	–	–	1.026	10.71
3	0.238	2.902	0.482	1.000	0.399	2.122
5	0.169	1.636	0.203	0.483	0.0972	0.480
8	0.123	0.945	0.116	0.324	0.0302	0.138
12	0.110	0.644	0.0636	0.148	0.0226	0.103
20	0.107	0.494	0.0465	0.196	0.0196	0.0743
Errors for Angular Scattering Curve II						
1	0.567	1.377	–	–	0.567	1.377
3	0.349	0.619	0.448	0.967	0.304	0.765
5	0.341	0.652	0.355	0.738	0.182	0.429
8	0.340	0.472	0.347	0.627	0.180	0.423
12	0.340	0.644	0.339	0.547	0.179	0.364
20	0.340	0.462	0.332	0.497	0.179	0.352
Errors for Angular Scattering Curve III						
1	0.971	5.231	–	–	0.971	5.231
3	0.178	1.077	0.479	1.013	0.217	0.635
5	0.123	0.540	0.211	0.486	0.168	0.421
8	0.0878	0.245	0.126	0.453	0.168	0.430
12	0.0866	0.218	0.0702	0.132	0.167	0.396
20	0.0865	0.225	0.0540	0.0961	0.167	0.391

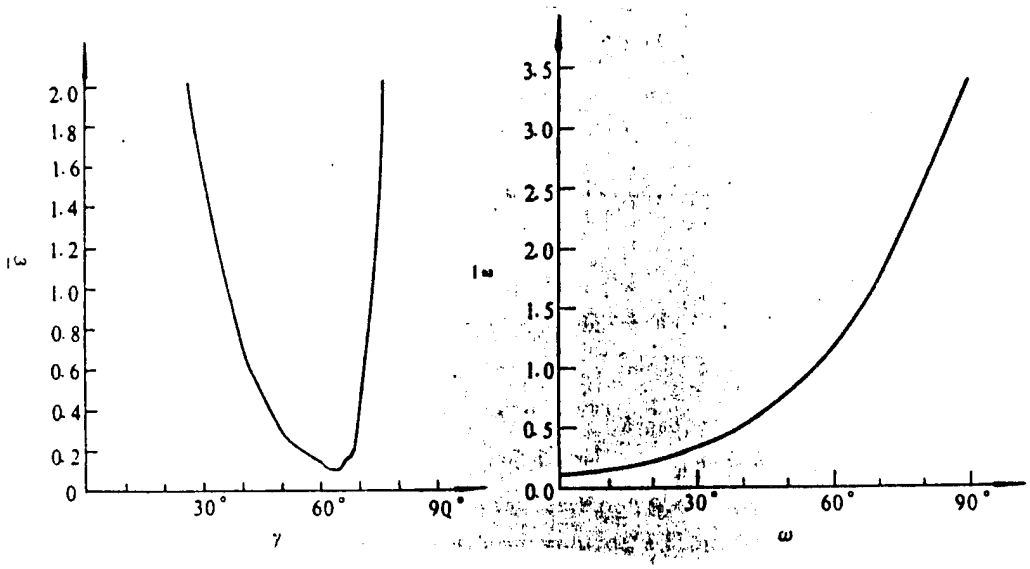

uncertainty in laser directions by using Eqs. (15) and (16) to estimate the test laser power with five to eight sensors uniformly deployed about 1km from the laser light source in tests. Such measured and estimated accuracies can satisfy the requirements for arms control inspections.

The first draft was received on February 19, 1993; the final revised draft was received for publication on July 5, 1993.

REFERENCES

[1] Foley TM. U.S, Soviet Scientists Propose System to Monitor Laser Asats. Aviation Week & Space Tech, 1989, May 15 : 31.

[2] Braid TH et al. Laser Brightness Verification. Science & Global Security, 1990, 2 : 59 ~ 78.

[3] Ruby RH et al. Laser ASAT Test Verification. New York : Federation of American Scientists, 1991, 1 ~ 102.

[4] McCartney EJ. 大气光学，分子和粒子散射. 北京：科学出版社，1988, 162.

[5] Drisoll WG. Handbook of Optics. New York : McGraw－Hill Book Company, 1978, 14 : 9.

[6] Zuev VG. Laser Beam in the Atmosphere. New York : Consultants Bureau , 1982, 148.

DISTRIBUTION LIST

DISTRIBUTION DIRECT TO RECIPIENT

ORGANIZATION	MICROFICHE
B085 DIA/RTS-2FI	1
C509 BALL0C509 BALLISTIC RES LAB	1
C510 R&T LABS/AVEADCOM	1
C513 ARRADCOM	1
C535 AVRADCOM/TSARCOM	1
C539 TRASANA	1
Q592 FSTC	4
Q619 MSIC REDSTONE	1
Q008 NTIC	1
Q043 AFMIC-IS	1
E404 AEDC/DOF	1
E410 AFDTC/IN	1
E429 SD/IND	1
P005 DOE/ISA/DDI	1
1051 AFIT/LDE	1
PO90 NSA/CDB	1

Microfiche Nbr: FTD95C000760
NAIC-ID(RS)T-0513-95